SOME EXPERIENCES USING WIND-TUNNEL MODELS IN ACTIVE CONTROL STUDIES

Robert V. Doggett, Jr., Irving Abel, and Charles L. Ruhlin
NASA Langley Research Center

SUMMARY

A status report and review of wind-tunnel model experimental techniques that have been developed to study and validate the use of active control technology for the minimization of aeroelastic response are presented. Modeling techniques, test procedures, and data analysis methods used in three model studies are described. The studies include flutter mode suppression on a delta-wing model, flutter mode suppression and ride quality control on a 1/30-size model of the B-52 CCV airplane, and an active lift distribution control system on a 1/22-size C-5A model.

INTRODUCTION

Dynamic and aeroelastic wind-tunnel models have played an important role in the development of aircraft and space technology. In many instances model tests are the most economical means, both in terms of time and cost, of determining needed data as compared to other methods such as analysis and flight tests. Models can be used to obtain results at conditions where analytical results are known to be inaccurate, for instance, transonic speeds. Ordinarily model results can be obtained in a more timely manner than flight results, and model tests are more amenable to conducting extensive parametric studies than are flight tests. Aviation applications of dynamic models have included such diverse areas as flutter, gust response, and landing loads while space application includes, among others, launch vehicle buffeting and ground wind load studies. Some of the many uses of models in aerospace applications are described in references 1 and 2, for example. Perhaps the extensive use of models is best illustrated by the fact that a literature search under the category of dynamic models gives a listing of over 2500 publications. This continued use of models has resulted in modeling technology reaching a rather advanced state of development. However, new technology and advanced concepts are continually being developed which offer new challenges to modeling technology. Active control technology is one of the latest challenges.

The addition of active controls to models adds a new complexity to modeling technology. In particular, control surface and actuation systems must be miniaturized, usually under severe weight restrictions, and new testing techniques must be developed.

The NASA Langley Research Center has embarked on a research program to develop experimental techniques so that wind-tunnel models can be employed to study and validate active control systems used to minimize aircraft aeroelastic response. Although the major thrust of this work is experimental, considerable emphasis is also being placed on the development of analytical techniques. This paper presents a status report and review of the experimental work that has been accomplished to date. An earlier status report is presented in reference 3. Some experiences in the testing of three different models in the Langley transonic dynamics tunnel are reported herein. In addition to presenting some basic experimental results from the three studies, such topics as model design and construction, active control system implementation, and wind-tunnel test techniques are discussed. Some comparisons between model experimental results and analysis are made, and in one instance some comparisons between model and flight test results are presented.

The first model program is a flutter suppression study using a delta-wing model. This research model, which is a simplified representation of a contemporary supersonic transport design, was used to develop basic flutter suppression modeling technology and to evaluate the aerodynamic energy flutter suppression concept developed by Nissim in reference 4. In addition to the results presented in reference 3, some later data obtained by using the delta-wing model are presented in reference 5. The second model study used a 1/30-size dynamically scaled aeroelastic model of the B-52 control configured vehicle (CCV). Both flutter mode control (FMC) and ride quality control (RQC) systems were implemented in this model study which was done in cooperation with the Air Force Flight Dynamics Laboratory. Some B-52 model flutter suppression results are given in reference 6. The Boeing Company, Wichita Division, has provided contractual assistance during both the delta-wing and B-52 model studies. The third model study was also done in cooperation with the Air Force and used a 1/22-size C-5A model. Under contract to the Air Force, the Lockheed-Georgia Company designed and built the model, and provided technical support for the wind-tunnel tests. The model was equipped with an active lift distribution control system (ALDCS) which used active controlled ailerons and horizontal tail to redistribute the dynamic wing loading in order to decrease the wing root bending moment. This C-5A model study was performed in conjunction with the development of a proposed lift distribution control system for the full-scale aircraft. The evolution of the proposed aircraft system is described in reference 7.

DELTA WING FLUTTER SUPPRESSION STUDY

General

The delta-wing model study was the first active control flutter suppression study undertaken at the Langley Research Center. In general, this program was initiated to develop the basic technology required for active control modeling studies and, in particular, to demonstrate experimentally that flutter can be suppressed by using active controlled aerodynamic surfaces. The flutter suppression concept chosen for implementation was the aerodynamic energy method

developed by Nissim (ref. 4). Simply stated, this aerodynamic energy concept says that flutter cannot occur if, for all allowable oscillatory motions, positive work is done by the wing on the surrounding airstream. That is, energy is transferred from the wing to the airstream.

A photograph of the delta-wing model mounted in the transonic dynamics tunnel is presented in figure 1, and model geometry is shown in figure 2. The 1.28 aspect ratio model planform was a cropped delta with a leading-edge sweepback angle of 50.5°, a taper ratio of 0.127, and a circular arc airfoil section with a thickness-to-chord ratio of 0.03. Two high-fineness ratio bodies were mounted on the wing lower surface to simulate engine nacelles. The model was cantilever mounted to a rigid mounting block that was bolted to the tunnel sidewall. The mounting block was enclosed in a simulated fuselage fairing which extended ahead of and behind the wing. This mounting arrangement brought the wing root outside of the tunnel wall boundary layer. The model was equipped with leading- and trailing-edge aerodynamic control surfaces. The controls were actuated by an electrohydraulic system which was controlled by a feedback system that was implemented on an analog computer located in the tunnel control room.

Design and Construction Considerations

Design.- Since the delta-wing study was of a research nature, it was not necessary that the model scale any particular full-scale airplane wing. However, for research studies to be as relevant as possible, it is desirable that the models used be representative of current or proposed configurations. Consequently, the delta-wing model design was based on a contemporary supersonic transport configuration. In particular, this model was a simplified 1/17-size version of the Boeing 2707-300 configuration. The design objective was to have a model that had similar flutter characteristics to those of the prototype and would flutter well within the operating boundary of the transonic dynamics tunnel. Other constraints to the model design were that the construction technique was to be as simple as practical and that construction cost was to be kept to a minimum. In developing the delta-wing final design, some preliminary wind-tunnel studies were made by using different size models that differed from one another in stiffness and mass properties. Some results of this study are reported in reference 8. From the results of this study a final design was selected. The flutter boundary of the final design (called configuration C in ref. 8) is very similar to the boundary (for one weight condition) of a rather expensive dynamically scaled replica-type model of the prototype configuration when both sets of data are scaled to airplane values.

Construction.- The construction of the delta-wing model was relatively simple. The basic structure was an aluminum alloy insert which tapered in thickness in the spanwise direction. Portions of the insert were chemically milled to simulate spars and ribs. The insert was covered with balsa wood that was contoured to give the desired airfoil section. The balsa wood was covered with one layer of fiber glass cloth which was doped to the wood. The two engine nacelles were made of steel tubing with balsa wood nose and tail streamlining fairings. The nacelles were ballasted with lead weights to give

the desired mass and inertia properties. Relative to the basic wing structure, the nacelles were rigid. The fuselage fairing was constructed of wood. The basic structure of the leading- and trailing-edge control surfaces was a metal tubing axle with balsa wood bonded to the axle. Two hardwood ribs were incorporated in each surface to provide additional chordwise stiffness. Each control surface was covered with a thin sheet of fiber glass cloth that was doped into place.

Flutter Suppression System

The flutter suppression system implemented on the delta-wing model was based on the aerodynamic energy concept described in reference 4. The implementation of this method used both leading-edge and trailing-edge control surfaces. The deflections of these control surfaces are related to the dynamic motions of the wing through a control law which relates control surfaces rotations to wing displacement and rotation. The resulting matrix equation is shown in figure 3. The elements of the C and G matrices are real numbers whose magnitudes are determined by aerodynamic energy considerations. In theory it is possible to determine values of the C and G matrix elements so that for all allowable wing motions energy is always transferred from the wing to the surrounding airstream and flutter cannot occur. However, in practice it is not necessary that flutter be precluded from occurring at all flight conditions, but only that the flutter speed be increased by some predetermined amount. That is, flutter cannot occur within some specified flight envelope.

Control laws.- Three different control laws were used for the delta-wing model. The three control laws are shown in figure 4. The first two (A and B) used both leading-edge and trailing-edge control surfaces. Control Law C used only a trailing-edge surface. Since the initial part of the study was aimed at demonstrating the basic aerodynamic energy concept, the first control law (Control Law A) used was that given in reference 4. The values used for the C and G matrix elements were the same as those Nissim developed by using two-dimensional unsteady aerodynamic theory. Control Law B was similar to the first except that three-dimensional unsteady aerodynamic theory (doublet lattice method) was used to determine the terms in the C and G matrices. Control Law C was also developed by using three-dimensional aerodynamics, but used only the trailing-edge control surface. In implementing both Control Laws B and C on the model, some difficulties were encountered. In effect, the system was so sensitive that if the model was disturbed in still air the control surfaces would begin to oscillate and drive the model. The exact reason for this problem has not been determined, but it is believed to be due to inertia coupling between the control surface and the wing portion of the model. This difficulty was cured by compromising the analytical values for the coefficients in the G matrix. The original G matrix values are shown in parentheses in figure 4. Analytical study results indicated that the required adjustment in G matrix values had little effect for Control Law C. However, for Control Law B there was a considerable degradation of the expected flutter dynamic pressure increase when the G matrix values were decreased. However, Control Law B still gave better performance in terms of increase in flutter dynamic pressure than that calculated for Control Law A.

Implementation.- Some of the physical components of the flutter suppression system are shown in the photograph presented in figure 5. A simplified block diagram of the system is presented in figure 6. The wing motion was sensed by two accelerometers that were located in line with the inboard edges of the control surfaces. The accelerometers were located at 30 and 70 percent of the chord. The accelerometer output signals were fed through signal conditioning equipment to an analog computer which was located in the tunnel control room. The aerodynamic energy control law was programed on the analog computer. The integration and differencing operations required to process the acceleration signals were also programed on the computer. (A portion of the analog computer may be seen in the upper left of figure 5.) The analog computer processed the accelerometer signals to determine appropriate actuator command signals. Command signals were passed to hydraulic servovalves which were mounted in the fuselage fairing at the model root. The servovalves controlled the supply of hydraulic fluid to miniature actuators that were mounted in the model at the inboard edge of each control surface. Control surface angular position was determined by using miniature silicon solar cells attached to each actuator shaft. Hydraulic and electric lines were routed to the actuators and sensors in trenches cut into the balsa wood which covered the aluminum insert. The model was also equipped with several resistance wire strain-gage bridges which were used to monitor model response. Although it is not indicated in figure 6, provision was provided for introducing external command signals to the control surfaces. External command signals to the trailing-edge surface were used for performing frequency sweeps and could be introduced with the flutter suppression system either operating (closed-loop) or not operating (open-loop).

Control surface actuators.- Initially it was decided to mechanize the control actuation system with an electromechanical system. The original concept was to mount an electric torque motor external to the model (inboard of the model root) and transmit the torque to the control surface by mechanical shafting. Considerable design effort with accompanying laboratory experimentation was expended in trying to come up with a satisfactory electromechanical system with little success. The major difficulty was associated with the shafting which had to exhibit little wind-up yet be light weight and not contribute any appreciable increase in stiffness to the basic wing. Finally, it was decided to switch to a hydraulic actuation system with the actuators located in the model at the control surfaces. Since no miniature hydraulic actuators existed that were small enough to fit within the model aerodynamic contour and provide the required torque, not to mention the light weight requirement, it was necessary to design and fabricate special actuators. The actuator design and fabrication is described in reference 9. The actuator is essentially a closed compartment that is separated into two chambers by a vane which rotates on a shaft that attaches to the control surface axle. The amount of shaft rotation is determined by the difference in hydraulic pressure between the two chambers. The actuator weighs 56.7 grams (0.125 lb) and is capable of providing a 4.52 N-M (40 in-lb) torque output with a 6.9×10^3 kN/m^2 (1000 lb/in^2) supply pressure over the frequency range from 0 to 25 Hz. A photograph of an assembled actuator attached to the trailing-edge control surface is presented in figure 7. The development of these miniature actuators represents a significant contribution to active control modeling and is not

limited to the delta-wing model application. In fact, similar actuators were used in the C-5A study to be discussed later in this paper. It was also necessary to design and fabricate special control-surface position indicators. Here again the space available was one of the most significant design constraints. The new position sensor (ref. 9) is a rather simple device that uses two silicon solar cells that are mounted on a common base that is attached to the actuator shaft. The solar cells are illuminated by a stationary light source. The intensity of the illumination changes as the shaft rotates, and a voltage is produced which is linearly proportional to the tangent of the shaft rotational angle.

Control surface location.- Since the specific aerodynamic energy control law developed in reference 4 was based on two-dimensional unsteady aerodynamic theory, it was necessary to conduct an analytical study to determine an appropriate location for the control surfaces. This study is described in reference 10, and some of the results are shown here in figure 8. Three possible control surface locations were considered as well as different locations of the model motion accelerometer sensors. In all cases the accelerometers were located at 30 and 70 percent of the local chord. The combination of control surface and sensor locations used for the delta-wing model was the midspan surfaces with the accelerometers alined with the inboard edge of the surfaces. This combination gave the second best increase in flutter dynamic pressure. The most improvement was obtained for outboard control surfaces and outboard sensor locations, but the use of this combination would have been very difficult since the wing was very thin in this region. It should be pointed out that the mathematical model used to generate the data presented in figure 8 was slightly different from the final delta-wing model so the expected flutter dynamic increase for the model would not be expected to be exactly those shown in the figure.

Test Techniques

Wind tunnel.- As was the case for all of the model studies described in this paper, the delta-wing model was tested in the Langley Research Center transonic dynamics tunnel. This facility is specially designed for and almost totally dedicated to the testing of dynamic aeroelastic models. The closed-circuit, single-return tunnel has a 4.88-m (16-foot) rectangular test section with flow expansion slots in all four walls. The tunnel flow conditions are continuously controllable over the Mach number range from about 0.07 to 1.2 at total pressures from near vacuum to slightly above one atmosphere. Either air or freon may be used as the test medium. All results reported herein were obtained by using freon.

Subcritical response.- In active flutter suppression studies it is not only desirable to determine actual flutter data points, but it is also necessary to determine stability information at conditions below the flutter boundary. The desired information is the damping of the critical flutter mode. Two techniques have been used with considerable success for determining subcritical damping levels. Both methods are based on the assumption that the response is that of a single-degree-of-freedom system. The first technique is

based on the procedure described in reference 11 and is referred to as "randomdec." Unlike most subcritical response procedures, randomdec does not require that the system be excited by special shakers, but depends on flow turbulence to supply the necessary input. The randomdec method is illustrated schematically in figure 9. The system response is assumed to be composed of three components - the responses to a step, to an impulse, and to a stationary random force. The system response to a step force is obtained by an ensemble average of a number of time sweeps, since the response to an impulse and to a random force average to zero. The time averaging was accomplished by using a small special-purpose computer. In the implementation here the different time segments were averaged sequentially. That is, the computer processed all the results for one time sample before beginning to collect the average data for the next sample. The averaging process for each time sample was started when the output signal reached a predetermined level. The model sensor output was passed to a gating circuit. When the preset signal level was reached, the gate was opened and the signal passed to the computer and averaged with values from previous samples. Electronic filters were used to isolate the frequencies of modes of interest. The averaged signal has the appearance of the damped oscillation of a single-degree-of-freedom system. The system damping is obtained from this decaying oscillation. Although the randomdec method has been used quite successfully in many cases to determine subcritical damping level, the method is not free from problems. Two difficulties are worthy of mention here. The first is noise contamination of the signal. At low levels of flow turbulence, the output of the model response sensor is relatively low. However, since the electronic noise level is independent of sensor output, the signal-to-noise level is relatively low and the result is low-quality decay signatures. Fortunately, this difficulty is most severe at conditions removed from the flutter condition. As the flutter condition is approached the system response naturally increases and the signal-to-noise level increases. The second problem is when there are two or more structural frequencies in close proximity to one another. Although signal filtering is useful, it is very difficult to completely filter out the unwanted mode. Although the band-pass filter is set for a very narrow range of frequency, the signal level outside the band is not completely attenuated because of filter roll-off. This results in a beat occurring in the randomdec decay signature and makes determining quantative values of the damping difficult. The decay looks like that of a coupled two-degree-of-freedom system.

The second technique, described in more detail in reference 12, requires the measuring of the forced response of the model. This method is illustrated schematically in figure 10 and will be referred to as the Co-Quad method. The model is excited by a sinusoidal force of varying frequency and the corresponding dynamic response is measured. Special electronic equipment is used to resolve the response into in-phase (called Co for coincident) and out-of-phase (called Quad for quadrature) components relative to the sinusoidal command signal. The damping of the system is obtained for each structural mode from the variation of the coincident component transfer function with frequency. Each resonant condition is treated as if it were that of a single-degree-of-freedom response, and the damping is obtained by using the formula shown in the figure. For active control models the Co-Quad method is easily implemented since an active controlled aerodynamic surface can be used to provide the

sinusoidal force input. For the delta-wing model frequency response data were obtained by oscillating the trailing-edge control surface. Co-Quad response data were obtained in terms of the ratio of accelerometer output $\ddot{h}_1$ to command signal $\delta_{t,c}$ to the trailing-edge control. The difficulties encountered with this method were similar to those described for the randomdec method, namely, noise and closely spaced resonant frequencies. However, in contrast to randomdec, the noise in this case is not primarily instrumentation noise but is the random response of the model which is superimposed on the sinusoidal response. The Co-Quad method requires a longer data gathering period than the randomdec technique. Typically about 30 seconds were required for randomdec while the Co-Quad frequency sweeps of about 4 minutes were used. The Co-Quad method is somewhat dangerous to use at conditions very near the flutter condition since the addition of the sinusoidal force to a model that already has significant response results in extremely large amplitudes as the forcing frequency sweeps through the critical flutter mode.

For the delta-wing model both the randomdec and Co-Quad methods were successfully used. In general, the randomdec method appeared to be the better of the two methods. The randomdec results, as judged by the qualitative appearance of the randomdec decay signature, appear to get better as flutter condition is approached. In contrast the Co-Quad method appeared to give the best results the farther you were away from the flutter condition. Where damping data were obtained by using both methods, the results were within what would be expected to be the experimental scatter band.

Results

Flutter.- Flutter studies of the delta-wing model were conducted at Mach numbers M of 0.6, 0.7, 0.8, and 0.9. Tests were performed both with (closed-loop) and without (open-loop) active controls. For the open-loop studies the control surfaces were kept at 0° deflection by applying hydraulic pressure to the actuators. The pressurized system acted as a stiff spring to keep the rotational frequency of each control surface many times higher than the wing flutter frequency. Once the open-loop flutter boundary of the wing was established, an evaluation of the effects of each of the three control laws on raising the boundary was made. However, studies for Control Laws A and B were restricted to $M = 0.9$ because of a high-frequency, large-amplitude oscillation of the leading-edge control. This phenomenon occurred around 65 Hz, as compared to the flutter frequency of from 11 to 12.5 Hz. It is believed that oscillatory motion was introduced in some manner by the mechanization of the leading-edge control, and was not a consequence of the control law, since the motion was also observed to a lesser degree with the control loop open.

A comparison of calculated and experimental results showing the effect of each control law on raising the open-loop flutter boundary is presented in figure 11. The results are presented in terms of percent increase in dynamic pressure at $M = 0.9$. By using Control Law A a 12-percent increase in dynamic pressure was obtained. The observed flutter motions for both open- and closed-loop operations were similar. The calculated increase for Control Law A is in excellent agreement with the experimental values. An earlier analytical

treatment for this control law was reported in reference 3 and showed a 21-percent increase in the flutter dynamic pressure. The differences between theory and experiment in reference 3 were attributed in part to the inability of the aerodynamic theory to adequately predict control surface pressure distributions. Early in the design of the delta-wing model static hinge-moment measurements were made to aid in the design of the control actuators. It is shown in reference 13 that the calculated values of hinge moment are somewhat higher than those that were measured. For the present analytical investigation the theoretical unsteady aerodynamic forces for the leading- and trailing-edge control surfaces were adjusted to take into account the differences between measured and calculated static hinge moments. The analytical results for Control Law B indicate a predicted increase of 24 percent. The experimental results demonstrate a minimum increase of 22 percent. Experimental results for Control Law B do not represent a closed-loop flutter point since further increases in dynamic pressure were restricted by the high-frequency oscillation of the leading-edge control surface mentioned earlier. Of the three control laws investigated, the largest increase in flutter dynamic pressure was obtained with Control Law C. A minimum increase in dynamic pressure of 30 percent was obtained with this control law. The model was not tested to the closed-loop flutter condition since the goal for these tests was set at a 30-percent increase in dynamic pressure assuming that closed-loop flutter was not encountered. The analytical results indicate a 34-percent increase.

The effectiveness of Control Law C in suppressing the flutter motion is vividly demonstrated by the time history of the wing bending strain-gage output shown in figure 12. Time is increasing from left to right. The tunnel dynamic pressure was slowly increased until open-loop flutter occurred (see left of figure). At this point the flutter suppression system was turned on as is indicated by the vertical dashed line on the right side of the figure. Note that when the system is turned on, oscillatory flutter motion is rapidly damped to a closed-loop no-flutter condition. The degree of confidence in the control system was such that when open-loop flutter was encountered, the active control loop was closed to suppress the motion.

In order to evaluate the active control system at other Mach numbers, Control Law C was both analytically and experimentally studied from $M = 0.6$ to $M = 0.9$. The results obtained are presented in figure 13 in terms of the variation of flutter-speed-index parameter with Mach number. The experimentally measured open-loop flutter boundary and the closed-loop no-flutter points for each Mach number are presented. At $M = 0.8$ a 9.4-percent increase in flutter-speed-index (20 percent in dynamic pressure) is shown. Unfortunately, at this point the model was damaged due to saturation of the closed-loop system because of limited available actuator angles ($\pm 9°$). Saturation caused the analog computer amplifiers to overload and forced the control surface to go hard against its stop resulting in open-loop flutter. The model was repaired and tested at Mach numbers of 0.7 and 0.6. A modest increase in flutter-speed-index of 5.7 percent (12 percent in dynamic pressure) was demonstrated at these two Mach numbers.

A comparison of calculated and experimental results (Control Law C) is also presented in figure 13. The calculations for the open-loop system show reasonable agreement at all Mach numbers.

Subcritical response.- Some subcritical response data obtained by using the Co-Quad technique are presented in figure 14 for a Mach number of 0.90. Both the in-phase and out-of-phase response in terms of the ratio of accelerometer output $\ddot{h}_1$ to trailing-edge command signal $\delta_{t,c}$ are presented. The curves on the left of figure 14 represent the model for open-loop operation at a dynamic pressure approximately 5 percent below the open-loop flutter boundary. The curves to the right in this figure show the model closed-loop response (Control Law C) at the open-loop flutter dynamic pressure. A qualitative measure of the active controls in reducing the forced response of the system is evident by the reductions in peak amplitudes around the flutter frequency of 11 Hz. Also shown in figure 14 are calculated response data. Note that the analysis does predict well the general behavior of the response. For these calculations, the effectiveness of the trailing-edge control was reduced by the ratio of measured-to-calculated static hinge moments.

B-52 MODEL STUDY

General

The planned B-52 model program includes studies in four active control areas. These areas are flutter mode control, ride quality control, maneuver load control, and relaxed static stability. To date a portion of the planned flutter mode control (FMC) and ride quality control (RQC) tests have been completed. The completed flutter suppression and ride quality control wind-tunnel tests are described herein. The flutter mode control portion of the model program is being conducted in cooperation with the Air Force Flight Dynamics Laboratory with contractual support being supplied in all four areas by The Boeing Company, Wichita Division.

The B-52 model program actually began in the late 1960's when a 1/30-size dynamically scaled aeroelastic model of the B-52E aircraft was constructed for use in symmetric gust studies in the transonic dynamics tunnel. Although provision was provided for incorporation of active controlled midspan ailerons and elevator in this original model, only gust response studies without active control were conducted. The results from these tests are not published. With the initiation of the B-52 CCV airplane program, it was decided to convert the B-52E model to a model of the CCV aircraft and expand the model program to include the four active control areas mentioned above. The B-52 CCV airplane program is described in reference 14, and some flight results are presented in reference 15. These CCV model tests offer the unique opportunity of validating wind-tunnel model techniques since flight data would be available for comparison with the model results. Although some modifications to the structural stiffness and mass were required in converting the original model to a CCV model, most of the modifications were associated with the installation of new aerodynamic control surfaces which included outboard ailerons, flaperons, and a pair of fuselage-mounted horizontal canards. A photograph of the complete free-flying model mounted on the two-cable suspension system in the transonic dynamics tunnel is presented in figure 15.

The objectives of the B-52 model wind-tunnel tests were to demonstrate the effectiveness of the FMC system and the RQC system, and to obtain data for correlation with analysis and airplane flight results. The design of the model systems was based on the corresponding CCV aircraft systems. The FMC system used active controlled flaperons and outboard ailerons. A pair of fuselage-mounted horizontal canard surfaces was used for the RQC system. The locations of the control surfaces are shown in figure 16. The feedback loops for both systems were implemented on an analog computer. The model control surfaces were actuated by using an electromechanical system.

Design and Construction

Scaling.- The B-52 model was a 1/30-size dynamically scaled aeroelastic model of the B-52 CCV airplane. The model weighed about 26 kg (57.75 lb) and had a wing span of 188 cm (6.16 ft). The model was designed to match the dynamic similitude parameters of reduced wavelength, mass ratio, and Froude number. Some of the scaling relationships and corresponding model/airplane flight conditions are presented in figure 17. Since the airplane flight conditions are at relatively low Mach numbers where compressibility effects are small, it was not considered necessary to match the Mach number between the airplane and the model. It is fortunate for the B-52 model study that flight conditions were at relatively low speeds since Mach number and Froude number scaling are difficult to satisfy simultaneously while still matching both reduced wavelength and mass ratio. A discussion of the conflicting requirements of Mach number and Froude number scaling is presented in reference 2.

Construction.- The construction technique used for the B-52 model was one that has been successfully used for a number of years in building aeroelastic models. Some details of the model construction are shown in figure 18. Aluminum alloy spars and beams were used to provide the basic stiffness of the wings and fuselage, respectively. Segmented pods constructed of wood frames covered with thin plastic sheets were attached to the spars and beams to provide the proper aerodynamic contour. The empennage was not elastically scaled. Both the horizontal and vertical tail were relatively stiff, but did have the proper total weight and center-of-gravity location. The engine nacelles were rigid streamlined bodies that had the proper inertia properties. The nacelles were attached to the wing spars by flexible beams which simulated the pylon stiffness. External fuel tanks were attached near the wings tips. The tanks were ballasted to simulate the mass that had to be added to the airplane to produce a flutter condition within the airplane operating boundary.

Test Techniques

Mounting system.- The B-52 model was mounted in the transonic dynamics tunnel by using a modified version of the two-cable suspension system described in reference 16. A portion of the cable support system is shown in figure 15. The model was supported by two cable loops, called flying cables, which were attached to the model at a common point. The cables were routed through low friction pulleys located on the tunnel walls. The forward cable loop was in the vertical plane, and the aft cable loop was in the horizontal plane. The

cables were kept under tension by stretching a soft spring in the rear loop. This mount system provided freedom for the model to translate laterally and vertically and to rotate about the pitch, roll, and yaw axes. In additon to the flying cables, four additional cables were attached to the model to provide emergency restraint (see fig. 15). These snubber cables extended out through the tunnel walls to a shock absorber system and a remotely controlled actuator. These cables were slack during normal test operations. The model was essentially flown in the tunnel test section on the mount system by a pilot located in the tunnel control room. For this model the pilot remotely operated the horizontal stabilizer to provide pitch control. For many models, external roll control is also provided, but this was not done for the B-52 model. Proper roll attitude (wings level) was obtained by manually setting small trim tabs located on each wing by a trial-and-error process. Once a satisfactory tab setting was obtained during the first test run, it was not necessary to change the setting for later runs.

For flutter model testing the primary mount system design requirements are that the model must be stable on the mount system, and that the frequencies of all rigid body modes must be well separated from the frequencies of the structural modes. For longitudinal ride quality control studies, there is the additional requirement that the short-period mode must be simulated as accurately as possible. Since the two-cable system introduces some spring restraints to the model that do not exist in free flight, the short-period mode is affected, and an additional rigid body mode (primarily a vertical translation mode) is added. In designing the B-52 model mount system, particular attention was given to properly simulating the airplane short-period mode and to keeping of the rigid body translational mode frequency as low as possible.

Flutter mode control (FMC).- For the most part the wind-tunnel test techniques used for the B-52 model FMC studies were the same as those used for the delta wing. Both the randomdec and Co-Quad subcritical response techniques were used. Some additional techniques were also used in an effort to determine subcritical damping from transient response data. In one technique the model was disturbed by sinusoidally driving the aileron and then abruptly removing the driving force to give a transient response. In another method a transient response was generated by driving the elevator with a one-cycle sine wave pulse. Neither of these two methods was very satisfactory for determining damping data since the transient response was almost, sometimes totally, obscured by the response of the model to tunnel turbulence. It is interesting to mention that transient response methods were satisfactorily used to determine damping during the B-52 CCV flight tests. Apparently the ratio of turbulence response to control surface input response was higher for the model than for the airplane. The lack of success with transient methods for the B-52 model does not mean that transient response damping determination techniques cannot be developed for model use, but rather means that more development work needs to be done.

Ride quality control (RQC).- Part of the RQC tests were accomplished by using an airstream oscillator system to provide a symmetric sinusoidal gust input to the model. The oscillating vane system consists of a set of biplane vanes installed on each side wall in the entrance cone to the tunnel test section. The vane system is shown in figure 19. The vanes are sinusoidally

oscillated (either symmetrically or antisymmetrically) through mechanical linkages by a hydraulic motor and flywheel arrangement. A vertical velocity component is induced in the flow in the center portion of the test section by the trailing vortices from the vane tips. The installation and early use of the vane system in the transonic dynamics tunnel is described in reference 17. The gust vane system has been calibrated and some typical results are presented in figure 20 in the form of a contour plot. The data shown are the variation of flow angle of attack with frequency and lateral position across the tunnel. Note that the gust angle decreases rapidly with increasing frequency and that there is some variation in flow angle with lateral position. Model response measurements were made with the RQS system on and off while the airstream oscillator system frequency was varied from 1 to 16 Hz. Also, frequency sweeps were made using external sinusoidal command signals to the model canards. The canard frequency was continuously varied over the frequency range from 4 to 24 Hz. Transfer functions were determined using the Co-Quad technique.

Active Control Systems

The B-52 model used active controlled outboard ailerons and flaperons for the FMC system. A pair of horizontal canards were used for the RQC system. The actuation systems for all of these surfaces were of the electromechanical type as opposed to the electrohydraulic system used on the airplane. The control surfaces were actuated by electric torque motors mounted in the model fuselage. The motors mechanically connected to the control surfaces through a rather complex mechanism of linkages. The complexity of the system can be seen by examining the photograph shown in figure 18. A more detailed description of the actuation system is presented in reference 10. The control laws were implemented and an analog computer located in the tunnel control room. Each control law was wired to a separate removable patch panel.

FMC system.- The design of the FMC system was based on the results of previous experience and analyses of the B-52 airplane. These results indicated that stabilizing aerodynamic forces are produced over the entire flutter oscillation cycle when the incremental lift generated by the control surfaces lags the wing displacement by 90°. Thus, the FMC feedback system was designed to produce the required phase lag between lift and displacement at the flutter frequency. The airplane FMC system is described in reference 18. A simplified block diagram of the model FMC system is presented in figure 21. The FMC system was redundant since there were two independent feedback loops. The first loop used the outboard ailerons as the active aerodynamic surfaces. Accelerometer signals from both the left and right wings were averaged and passed through a shaping filter to generate the aileron feedback command signal which was routed to the single aileron actuator. The flaperon loop was similar to the aileron loop except that each flaperon had its own actuator. In concept the model and B-52 CCV airplane systems are the same, the only difference is in the actuator dynamic characteristics. That is, a comparison of the two transfer functions would show a difference. However, over the frequency range of interest, the two actuators do have similar dynamic characteristics. Note that provision was provided at summing junctions (see upper left of fig. 21) for introducing external command signals to the actuators. The external command signals were used to

drive the control surfaces for model excitation. The command signals can be used when the FMC system is either operating (closed-loop) or not operating (open-loop).

RQC system.- The RQC system was designed to provide about a 30-percent reduction in the RMS vertical acceleration level at the pilot's station. A simplified block diagram of the RQS system is presented in figure 22. Pilot station acceleration signals are fed back through a shaping filter to produce the required canard command signals. In the RQC system it was necessary to add compensation to account for the differences in dynamic characteristics between the model and airplane actuators. The design of the model RQC system is described in reference 19.

B-52 Results

FMC system.- The primary objectives of the model FMC system studies were to establish the open-loop (FMC off) flutter velocity, to demonstrate the effectiveness of the closed-loop system (FMC on), and to obtain data for correlation with model analysis and full-scale flight tests.

During the FMC studies the open-loop flutter velocity was determined, and both open- and closed-loop subcritical response measurements were made above and below the open-loop flutter velocity. As described previously, several experimental techniques were used for determining the subcritical response characteristics. In general, the most useful results were from the forced response Co-Quad technique. Representative measurements of the in-phase and out-of-phase components of the wing acceleration $\ddot{Z}_{WBL\ 78.3}$ to aileron command displacement $\delta_{a,c}$ as a function of frequency are shown in figure 23. These results are approximately 6 percent in velocity below the measured open-loop flutter point. The curves to the left on this figure are the frequency response of the open-loop system; the curves to the right represent the closed-loop response. The effectiveness of the FMC in reducing the forced response of the system is readily apparent by comparing the resonant response peaks of the open- and closed-loop systems.

The randomdec technique worked best as the flutter speed was closely approached and the damping in the flutter mode became very small. It was especially useful here since it was considered hazardous to apply external excitation. A typical response time history trace for the right wing accelerometer $\ddot{Z}_{WBL\ 47.8}$, and the associated randomdec signature, taken approximately 3 percent in velocity below the flutter point, is shown in figure 24.

A comparison of calculated and measured flutter mode damping versus airspeed for the model is presented in figure 25. The measured values were obtained from the forced response technique while the calculated values were obtained from the characteristic roots of the equations of motion. The comparison shows the analysis to be conservative by about 10 percent in predicting the open-loop flutter velocity. This difference may be attributed in part to the fact that the measured structural damping of the model was somewhat higher than the damping used in the flutter analysis. Both experimental and analytical

results show that the FMC system provides a substantial increase in damping near the open-loop flutter velocity. The measured closed-loop data show the system to be less effective than analytically predicted. This difference is believed to be due to hystersis in the outboard aileron actuator system combined with a reduced effectiveness of the control surfaces that were not accounted for in the analysis. The maximum velocity tested with the closed-loop system was 48.3 m/sec (158 ft/sec); however, no damping values were measured above 47.2 m/sec (155 ft/sec) (indicated by a dashed line in fig. 25).

A comparison of measured flutter mode damping versus airspeed for the model and full-scale airplane is shown in figure 26 in terms of airplane velocity. The airplane damping values were obtained from transient response records. As indicated in this figure the model open-loop flutter speed is about 7.9 percent higher than the airplane flutter speed. This difference is attributed to minor variations in model mass and stiffness from the required values combined with some cable-mount effects on the rigid body dynamics of the model. The calculated airplane flutter speed was about 8.3 percent below the measured point. Thus a consistency does exist between measured and calculated flutter velocities for both the model and airplane in that the analysis was conservative in both cases by about the same amount. The data in figure 26 show that the model and airplane have the same closed-loop damping trends. In both cases the closed-loop system significantly increases the damping near the open-loop flutter velocity. Although some differences in damping level do exist, it is felt that the correlation between model and airplane is quite reasonable. As indicated in the figure, both the model and airplane were tested above the open-loop flutter velocity.

RQC system.- The objectives of the RQC studies were to demonstrate the effectiveness of a ride control system in reducing the acceleration at the pilot's station and to obtain data for correlation with analysis and full-scale flight. During the RQC studies the open-loop (RQC off) and closed-loop (RQC on) response of the model to external excitation was measured. The first series of tests that were performed involved measuring the response of the model to a sinusoidal gust field generated by the oscillating vanes. The frequencies of the primary modes of interest were at 2, 13, and 17.5 Hz. Sample results obtained from the in-phase and out-of-phase components of the pilot station acceleration $\ddot{Z}_{nose}$ as a function of vane frequency are presented in figure 27. The curves to the left are the open-loop response; the curves to the right, the closed-loop response. Attenuation of the closed-loop response around 2 Hz is apparent. However, the response in the 13-Hz mode is so low that the effect of the ride control system is not obvious. These results for the higher modes are due to the fact that the effectiveness of the oscillating vanes in generating the gust field falls off rapidly at the higher values of frequency (see fig. 20). The canard surfaces were used to generate the excitation for the higher modes. Results at the same test condition obtained from a canard frequency sweep are shown in figure 28. The canard amplitude was 2°. The data are presented for both the open- and closed-loop system in terms of the ratio of pilot station acceleration $\ddot{Z}_{nose}$ to canard command signal $\delta_{c,c}$ as a function of canard frequency. The effect of the RQC system on the higher modes is now evident. It appears that some combination of testing techniques is required to accurately define the system response curves.

C-5A ALDCS MODEL STUDY

General

In an effort to reduce wing fatigue damage and thereby prolong the service life of the C-5A fleet, the Air Force has contracted with the Lockheed-Georgia Company to develop and flight test a C-5A airplane with an active lift distribution control system (ALDCS). This system is designed to reduce the incremental inboard-wing stresses experienced during gusts and flight maneuvers. The ALDCS uses existing controls on the airplane - ailerons to unload the wing tips and elevators to keep the airplane in trim. Specific design goals for the ALDCS are to reduce the symmetric flight incremental wing root bending moment by at least 30 percent while limiting any increase in torsional moment to less than 5 percent. A detailed description of the airplane ALDCS is presented in reference 20.

A wind-tunnel study of a dynamically scaled aeroelastic model equipped with the proposed ALDCS was undertaken for the following objectives: (1) to determine the ALDCS effectiveness; (2) to investigate the adverse coupling of structural modes due to the ALDCS, particularly wing flutter; and (3) to obtain experimental data for correlation with analysis and to guide flight tests. A photograph of the 1/22-size model used in the study is presented in figure 29. The model program was a joint effort of the Air Force, the Lockheed-Georgia Company, and the Langley Research Center. The model study was performed concurrently with the development of the airplane ALDCS and was completed within a 9-month period prior to the beginning of airplane flight tests. Basically, the model program involved the modification of an existing 1/22-size flutter model to match Froude number scaling, the incorporation of the ALDCS in the model, and wind-tunnel tests in the transonic dynamics tunnel.

Some unique features of the C-5A model study were that it was the first scaled model study of a lift distribution control system, and the model had an onboard hydraulic system. This hydraulic system included pump, fluid cooling system, and servovalves that powered the control surface actuators. The weight of this system (about 16.3 kg or 36 lb) was absorbed as onboard cargo in the fuselage. The C-5A model study required the application of many specially developed wind-tunnel systems and model technologies such as (1) the two-cable suspension system for minimum restraint to permit the model to be essentially free-flying, reference 16; (2) although not used, a special roll control system was available which altered the mount system cable angles in case the aileron deflections needed to keep the model in roll trim because excessive, reference 21; (3) a lift-simulation (cable-pneumatic spring) device that provided the capability of varying the model lift coefficient for given test conditions, reference 22; (4) an oscillating vane system which generated sinusoidal gusts, reference 17; and (5) aileron actuators on the model wing which were basically duplicates of those developed for the delta-wing flutter suppression model previously described.

Model

Scaling.- Although a 1/22-size flutter model of the complete C-5A airplane was available from earlier flutter clearance studies in the transonic dynamics tunnel, the decision was made to rescale and modify the model to match the airplane Froude number. This allowed a closer simulation of the aerodynamic loading and dynamic characteristics of the airplane, thus, a better evaluation of the ALDCS could be made. For a Froude number scaled model, the mass ratio and reduced wavelength are also matched at the selected design test conditions. The model scaling factors were derived so that Froude number was matched for the model at a Mach number of 0.263 and a dynamic pressure 2.394 kN/m^2 (50 lb/ft^2) in the wind tunnel with freon as the test medium. The corresponding airplane flight conditions were a Mach number of 0.58 and a dynamic pressure of 19.87 kN/m^2 (415 lb/ft^2) which corresponded to an altitude of 1524 m (5000 ft). It was assumed that at these relatively low subsonic Mach numbers the compressibility effects were not important and that there would not be any significant differences between the aerodynamic characteristics of the model and the airplane.

Design and construction.- The C-5A ALDCS model was designed to scale two airplane configurations, wing fuel loadings of 0 and 33 percent with approximately 113 400 kg (250 000 lb) of cargo for both cases. The 1/22-size model had a wing span of 3.037 m (9.96 ft). The 0-percent fuel configuration weighed 65.1 kg (143.5 lb), and the 33-percent fuel configuration weighed 77.2 kg (170.2 lb). To minimize costs, components of an existing flutter model were used as much as possible in the ALDCS model. A spar and pod type of construction was used. Some of the construction details are shown in figures 30 and 31. The metal spars carried the structural loads and simulated the stiffness characteristics. The balsa wood pods duplicated the aerodynamic shape and were ballasted (with the spars) to simulate the mass characteristics. The ALDCS model required close simulation of the wing properties. Therefore, new wing spars, engine-pylon spars, and fuselage spars were constructed. (The fuselage signficantly affected the wing dynamics.) Some new wing and fuselage pods were also constructed. The existing flutter model empennage was used in the ALDCS model; consequently, the empennage stiffness was not properly scaled. In reworking the empennage to incorporate the horizontal tail active control mechanism, an attempt was made to simulate the required scaled mass properties of the overall empennage; however, the final empennage was considerably under weight. The ailerons were scaled and consisted of a metal spar covered with balsa wood which was faired to give the proper scaled aerodynamic shape. The aileron-wing gap was not sealed on the model, although the gap was kept as small as practical.

With the exception of the empennage, the model simulated the mass and stiffness of the airplane quite well, including the important wing structural mode frequencies and mode shapes. It was concluded that the model adequately represented the airplane for the purposes of the ALDCS study.

Control systems.- The aerodynamic surfaces used for active controls on the C-5A airplane consisted of the ailerons and the elevators. However, for practical model design considerations, the all-movable horizontal tail was used

to provide active pitch control instead of the elevators. An appropriate compensation was made in the control law to account for this difference.

All active control surfaces on the model were actuated by an onboard hydraulic system. The aileron actuators were of the same design as those used for the delta-wing research model described earlier. The aileron also could be remotely controlled (by the model pilot) to permit static roll trim control. The tail actuator controlled the dynamic pitch angle of the complete horizontal stabilizer and was simply a hydraulically actuated piston (see fig. 30). The piston housing was mechanically coupled to an electric motor drive system (also controlled by the pilot) which could move the complete piston unit and thus vary the tail static pitch angle for model pitch trim. The piston drove the tail dynamically and worked against two coil springs which attempted to keep the piston in a centered position. In the event of a hydraulic failure, the centering springs would keep the horizontal stabilizer at its static trim setting, whereas the ailerons would tend to become free-floating and self-alining with the wing countour.

The power for the hydraulic system was provided by an onboard hydraulic pump (see fig. 31). This pump was an aircraft system that was adapted to the model and had an output pressure of 11.3×10^3 kN/m^2 (1600 lb/in^2). For lengthy operation of the hydraulic system, it was necessary to cool the hydraulic fluid, and a water cooling jacket was provided onboard the model. The water was externally pumped to the jacket through flexible plastic hoses which were secured to the instrumentation umbilical cord.

Servovalves were used to control the hydraulic pressure supplied to the control surface actuators. These valves were of the same type as those used for the delta-wing model. The model actuation system was compensated by electronic circuitry to give frequency response characteristics that closely matched the transfer functions of the airplane actuators.

Instrumentation.- Bending and torsional moments on the model were measured by using resistance-wire strain gages mounted at several spanwise stations on the wings and at the roots of the vertical and horizontal tail surfaces. Aileron hinge moments were measured by using strain gages mounted on each aileron pivot arm. Vertical acceleration on each wing near the aileron and at the fuselage center of gravity was measured by using accelerometers. Fuselage angle of attack was measured by using a servoaccelerometer. The angular position of each control surface was measured by using potentiometers. Fuselage center-of-gravity pitch rate was measured by using a pitch rate gyro. Tension in the model support cables was measured by using load cells.

Control Law

A simplified diagram of the active control systems used in the C-5A ALDCS model is presented in figure 32. There were two active control systems operating on the model, the basic aircraft pitch stability autmentation system (pitch SAS) and the ALDCS. Both commanded symmetric actuation of the control surfaces. The pitch SAS employed a feedback from the pitch rate gyro at the

fuselage center of gravity to actuate the horizontal tail. The ALDCS employed feedbacks from both the pitch rate gyro and the fuselage center-of-gravity accelerometer to actuate the horizontal tail and feedbacks from the wing tip accelerometers to actuate the ailerons. Note that the acceleration signals from the two wings were summed in order to filter out unsymmetrical motions. The capability of supplying external command signals to the control surfaces was included. The gains K_{STAB}, K_{AIL}, and K_{SAS} were scheduled signal gains manually set according to a predetermined Mach number dynamic pressure schedule.

Tests and Procedure

A summary of the C-5A ALDCS model test configuration and test parameters is presented in figure 33. The 33-percent wing fuel configuration was tested first because this was a more realistic flight condition, and, hence, considerably more data were obtained with this configuration. The 0-percent fuel configuration, after a brief ALDCS effectiveness check, was extensively investigated to determine the ALDCS effect on flutter because this wing configuration had the lowest flutter speed (ALDCS off).

Model support and test techniques.- The free-flying mount system used for the C-5A model was essentially the same as that previously described for the B-52 model with the exception that the pulleys were mounted in the model fuselage rather than on the tunnel wall. The model was restrained by using the snubber cables during the flutter tests at Mach numbers above about 0.7 because the model was unstable in a Dutch roll type mode. During the dynamic load tests, the model was not only snubbed but was also tied down by cables attached to the nose and rear of the fuselage.

In the static aerodynamic studies, the simulated lift device shown in figure 34 was employed. Briefly, this device consisted of a single cable attached to the fuselage at the model center of gravity which would exert a down force to the model as needed. This was accomplished by attaching the cable to a piston essentially floating in an air cylinder which was located in the plenum outside of the test section. By varying the air pressure on the top side of the piston, a down load could be transmitted to the model. In operation, as the model angle of attack was varied, the air pressure to the cylinder was adjusted to compensate for the additional model lift and to maintain the model at its normal flying position near the center of the tunnel. By measuring the tension in the cable, the additional lift on the model could be measured.

Aileron and stabilizer frequency sweeps were extensively employed in the dynamics tests. In these sweeps, an external sinusoidal electrical signal was supplied to the control system to actuate symmetrically the control surfaces and generate aerodynamic forces. The model response to these aerodynamic excitation forces was measured. The frequency sweeps ranged from about 0.5 to 20 Hz. Several control surface amplitudes were used. Symmetric aileron and stabilizer step/ramp functions were also employed to excite the model. Part of the ALDCS effectiveness studies involved use of sinusoidal gusts generated by the tunnel oscillating vane system. Both symmetric and antisymmetric gusts were

used in the tests. The gust vane frequency was varied from 0.7 to 16 Hz. In order to reduce the static bending moments, a large portion of the tests were performed with the ailerons set at a nominal angle of +5° trailing-edge up (called uprig angle).

Static aerodynamic measurements.- With the model free-flying and the lift-simulation-device cable attached, static aerodynamic data were measured at dynamic pressures of 1.92 and 2.39 kN/m^2 (40 and 50 lb/ft^2). For each of the three aileron uprig angles of 0°, +10°, and -10°, the model was varied through the angle-of-attack range about the normal flying attitude. The added lift was compensated for by adjusting the down force in the lift cable. Thus, static aerodynamic data, such as model C_{L_α} and C_{L_δ}, and the effect of the aileron on the wing lift distribution could be derived.

Dynamic load measurements.- The purpose of these tests was to determine the dynamic wing and empennage loads produced by oscillating the ailerons and stabilizer. Data were obtained for aileron and stabilizer frequency sweeps at various amplitudes. During these tests the model was restrained by the snubber cables and tie-down cables at the nose and rear of the fuselage. This fuselage restraint was used in an effort to structurally uncouple the wing and empennage approximating a cantilever root condition so that the experimental data could be correlated with analysis where the wing and empennage were treated independently as cantilevered structures.

ALDCS effectiveness tests.- The ALDCS effectiveness tests were made with the model free-flying and a nominal aileron uprig of +5°. The effectiveness of the ALDCS in reducing wing loads was examined for a variety of test variables as shown in figure 33. An earlier version of the control law, identified by analysis as destabilizing a higher structural mode, was also tested.

Flutter tests.- The test procedure was to vary Mach number M and dynamic pressure q along an essentially constant total pressure line with the model ALDCS off. At discrete points along each constant pressure path, the model response to an aileron step was measured. The aileron step was repeated with the ALDCS on. These M-q sweeps were initiated at a low density level in the tunnel, and the sweeps repeated at higher density levels until the envelope was cleared or flutter was obtained. Because of a model Dutch roll type of instability on the cable mount, it was necessary to conduct a portion of the flutter tests with the model snubbed.

Results

The major objectives of the C-5A ALDCS model study were successfully accomplished. The model and the active control systems appeared reasonably representative of the airplane, and the model ALDCS achieved its design goal in reducing wing dynamic bending moment. However, because the model suspension system significantly distorted the rigid body modes, the effect of the ALDCS on these modes was not determined. The ALDCS effect on the model wing flutter characteristics appeared to be negligible, probably because the wing flutter

mode was antisymmetric, whereas the ALDCS was designed to attenuate symmetric loads only. Some typical results are presented in figures 35 to 38.

The model appeared to simulate reasonably well the overall static aerodynamic characteristics including wing load distribution of the airplane. However, the ailerons were not as effective as those of the airplane. A given model aileron deflection produced less (ranging from about 15 to 35 percent) of a load change than was produced on the airplane for the same deflection. Aileron gains of 1.6 times nominal were therefore included in the test parameters. The dynamic effects on the model loads due to the control surface oscillations compared favorably with analysis.

The ALDCS effectiveness was established best by the aileron frequency sweeps. The aileron sweeps excited higher frequency modes better than either the stabilizer sweeps or the sinusoidal gust sweeps. At the present time, the step/ramp response data have not been reduced sufficiently to determine their quality. The response of the model wing to a typical aileron sweep at the scaled flight condition is shown in figure 35. For these sweeps, the model scaled the 33-percent wing fuel configuration, the aileron amplitude was set for $\pm 5°$, the ALDCS was at nominal aileron gain, and the pitch SAS was on. The normalized wing bending moment at the wing root station is shown on the left plot; the normalized wing torsional moment is shown on the right. The frequency of the wing first bending mode was about 4 Hz. Another mode which contributed significantly to the model response had a frequency of about 11 Hz. It can be seen that the major effect of the ALDCS is to reduce the bending moments by about 50 percent at the 4-Hz mode; the torsional moments were also reduced by the ALDCS. The distribution of the bending and torsional moments along the wing span is shown for the same conditions in figures 36 and 37. In figure 36 the bending moments pertain to the 4-Hz mode. The torsional moment in figure 37 is for the 11-Hz mode where the torsional moments are greatest. It can be seen that the load reduction experienced at the root is obtained in nearly the same proportion over the entire span.

In the flutter tests, the 33-percent wing fuel configuration did not flutter within the scaled flight envelope. The 0-percent fuel configuration experienced antisymmetric wing flutter at the two points shown in figure 38. The data in this figure are presented in the form of airplane equivalent airspeed. In each instance, the ALDCS had no effect on the flutter. The model flutter occurred at a frequency of about 13 Hz and appeared to consist of a combined higher wing bending and torsional mode with most of the motion on the outboard portion of the wing. A similar type of wing flutter occurred during earlier flutter model tests.

CONCLUDING REMARKS

In this paper the experiences to date in testing aeroelastic models equipped with active controls in the Langley Research Center transonic dynamics tunnel have been described. Such items as model design, construction, and test techniques have been described in discussing three model experimental programs.

Also, some typical data results have been presented. The three model studies were a simple delta-wing flutter suppression model, a 1/30-size dynamically scaled aeroelastic model of the B-52 CCV, and a 1/22-size dynamically scaled aeroelastic model of the C-5A aircraft. The delta-wing model was used to evaluate the aerodynamic energy concept of flutter suppression. The B-52 model was equipped with flutter mode control and ride quality control systems, while the C-5A model was equipped with a lift distribution control system. In all three studies active controls were successfully implemented on the models. The delta-wing flutter suppression system did provide an increase in flutter dynamic pressure, and the experimental results are in reasonable agreement with analytical trends. Both B-52 model systems provided improved performance, and the FMC experimental results compare favorably with analytical and flight data. The C-5A ALDCS did provide a significant reduction in incremental dynamic bending moment on the wing with no apparent effect on the flutter characteristics.

Experiences with these models have indicated that the addition of active controlled aerodynamic surfaces has, indeed, added complexity to aeroelastic modeling technology. However, no insurmountable obstacles have been encountered in these three studies, and the success to date indicates that much useful information can be obtained from model test results.

REFERENCES

1. Proceedings of Symposium on Aeroelastic and Dynamic Modeling Technology, RTD-TDR-63-4197, Part I, Mar. 1964.

2. Regier, Arthur A.: The Use of Scaled Dynamic Models in Several Aerospace Vehicle Studies. Paper presented at the ASME Colloquium on the Use of Models and Scaling in Shock and Vibration (Philadelphia, Pa.), Nov. 1963.

3. Abel, Irving; and Sandford, Maynard C.: Status of Two Studies on Active Control of Aeroelastic Response. NASA TM X-2909, 1973.

4. Nissim, E.: Flutter Suppression Using Active Controls Based on the Concept of Aerodynamic Energy. NASA TN D-6199, 1971.

5. Sandford, Maynard C.; Abel, Irving; and Gray, David L.: A Transonic Study of Active Flutter Suppression Based on an Aerodynamic Energy Concept. Preprint 74-403, Am. Inst. Aeron. Astronaut., Apr. 1974.

6. Redd, L. T.; Gilman, J., Jr.; Cooley, D. E.; and Sevart, F. D.: A Wind Tunnel Study of a B-52 Model Flutter Suppression System. Preprint 74-401, Am. Inst. Aeron. and Astronaut., Apr. 1974.

7. Disney, T. E.; Hargrove, W. J.; and Eckholdt, D. C.: Historical Review of the C-5A Lift Distribution Control Systems. Paper presented at Symposium on Advanced Control Technology and Its Potential for Future Transport Aircraft, NASA (Los Angeles, Calif.), July 1974.

8. Sandford, Maynard C.; Ruhlin, Charles L.; and Abel, Irving: Transonic Flutter Characteristics of a 50.5° Clipped-Delta Wing with Two Rearward-Mounted Nacelles. NASA TN D-7544, 1974.

9. Bergmann, Gerald E.; and Sevart, Francis D.: Design and Evaluation of Miniature Control Surface Actuation Systems for Aeroelastic Models. Preprint 73-323, Am. Inst. Aeron. and Astronaut., Mar. 1973.

10. Severt, F. D.; Patel, S. M.; and Watlman, W. J.: Analysis and Testing of Stability Augmentation Systems. NASA CR-132349, 1973.

11. Cole, Henry A., Jr.: On-Line Failure Detection and Damping Measurement of Aerospace Structures by Random Decrement Signatures. NASA CR-2205, 1973.

12. Keller, Anton C.: Vector Component Techniques: A Modern Way to Measure Modes. Sound and Vibration, Vol. 3, No. 3, Mar. 1969, pp. 18-26.

13. Rainey, A. Gerald; Ruhlin, Charles L.; and Sandford, Maynard C.: Active Control of Aeroelastic Response. Presented to Stability and Control Panel of AGARD (Braunschweig, Germany), Apr. 10-13, 1972.

14. Kass, Gerald S.; and Johannes, Robert P.: B-52 Control Configured Vehicles Program. Preprint 72-747. Am. Inst. Aeron. and Astronaut., Aug. 1972.

15. Arnold J. I.; and Murphy, F. B.: B-52 CCV Flight Test Results. Paper presented at Symposium on Advanced Control Technology and Its Potential for Future Transport Aircraft, NASA (Los Angeles, Calif.), July 1974.

16. Reed, Wilmer H., III; and Abbott, Frank T., Jr.: A New "Free-Flight" Mount System for High Speed Wind-Tunnel Flutter Models. Proceedings of Symposium on Aeroelastic and Dynamic Modeling Technology, RTD-TDR-63-4197, Part I, Mar. 1964.

17. Gilman, Jr., Jr.; and Bennett, Robert M.: A Wind-Tunnel Technique for Measuring Frequency-Response Functions for Gust Load Analysis. Journal of Aircraft, Vol. 3, No. 6, Dec. 1966.

18. Hodges, Garold G.: Active Flutter Suppression - B-52 Controls Configured Vehicle. Preprint 73-322, Am. Inst. Aeron. and Astronaut., Mar. 1973.

19. Sevart, Francis F.; and Patel, S.: Analysis and Testing of Aeroelastic Model Stability Augmentation Systems. NASA CR-132345, 1973.

20. Hargrove, W. J.: The C-5A Active Lift Distribution Control System. Paper presented at Symposium on Advanced Control Technology and Its Potential for Future Transport Aircraft, NASA (Los Angeles, Calif.), July 1974.

21. Abel, Irving: Evaluation of a Technique for Determining Airplane Aileron Effectiveness and Roll Rate by Using Aeroelastically Scaled Models. NASA TN D-5538, 1969.

22. Rainey, A. Gerald; and Abel, Irving: Wind-Tunnel Techniques for the Study of Aeroelastic Effects on Aircraft Stability, Control, and Loads. Presented to Flight Mechanics Panel of AGARD (Marseilles, France), Apr. 21-24, 1969.

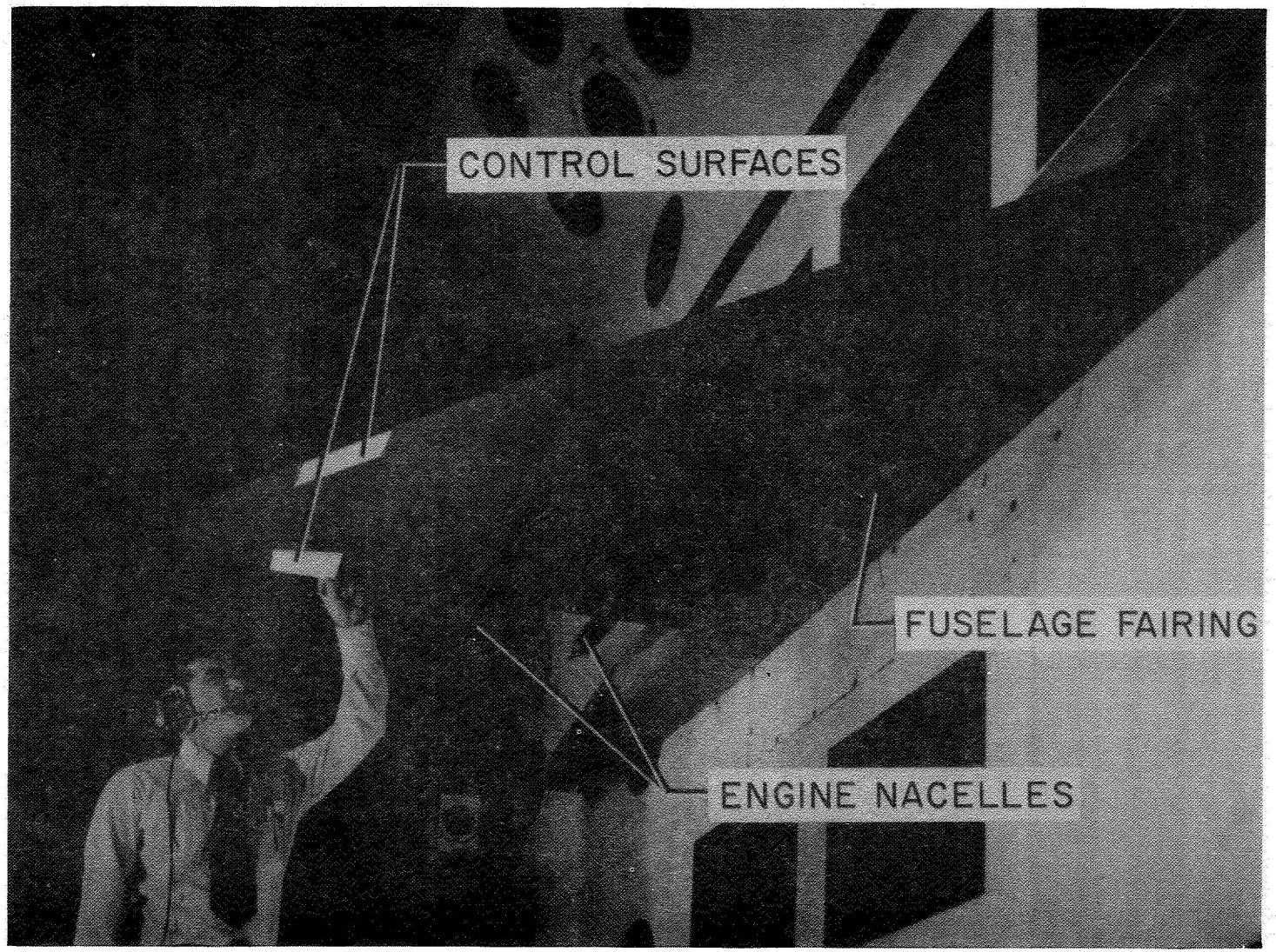

Figure 1.- Delta-wing model mounted in transonic dynamics wind tunnel.

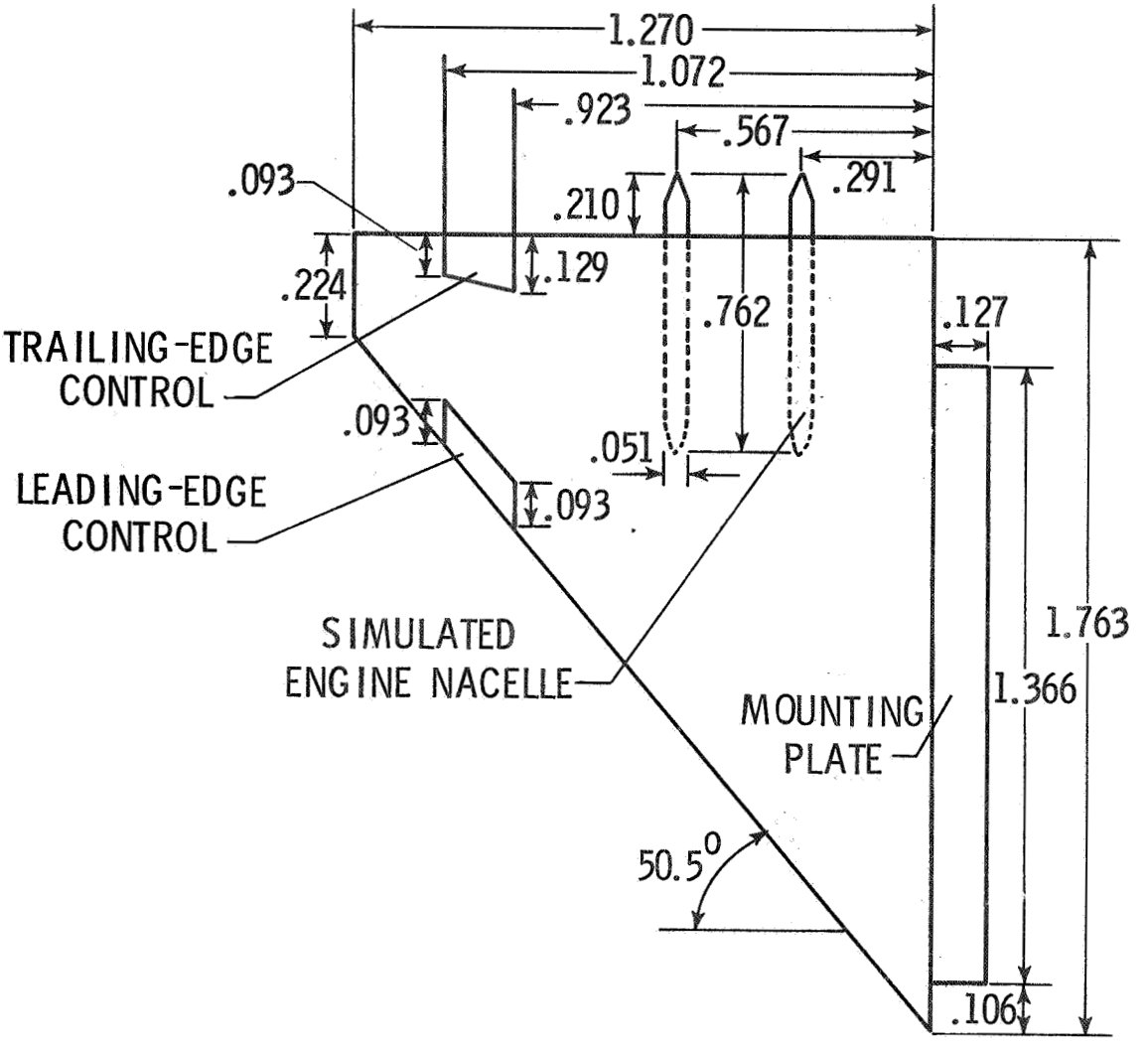

Figure 2.- Sketch of delta-wing model. (All linear dimensions are in meters.)

$$\begin{Bmatrix} \beta \\ \delta \end{Bmatrix} = \begin{bmatrix} C_{11} & C_{12} \\ C_{21} & C_{22} \end{bmatrix} \begin{Bmatrix} \frac{h_1}{b} \\ \alpha \end{Bmatrix} + i \begin{bmatrix} G_{11} & G_{12} \\ G_{21} & G_{22} \end{bmatrix} \begin{Bmatrix} \frac{h_1}{b} \\ \alpha \end{Bmatrix}$$

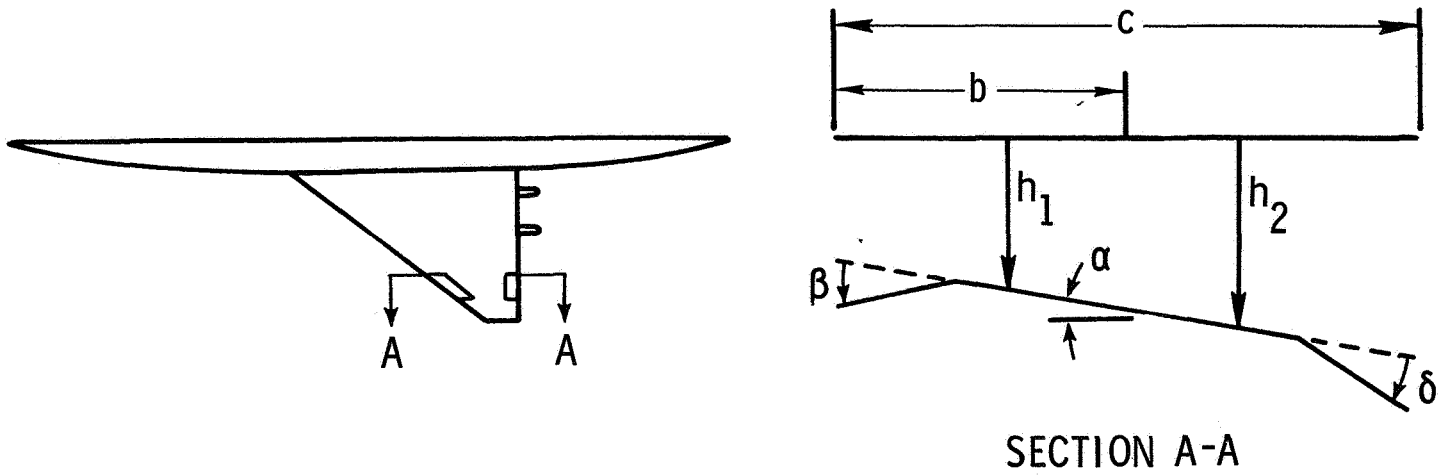

Figure 3.- Basic control law parameters.

$$\begin{Bmatrix} \beta \\ \delta \end{Bmatrix} = \begin{bmatrix} 0 & 5.6 \\ 0 & -1.4 \end{bmatrix} \begin{Bmatrix} \frac{h_1}{b} \\ \alpha \end{Bmatrix} + i \begin{bmatrix} 0 & 1.5 \\ .6 & .2 \end{bmatrix} \begin{Bmatrix} \frac{h_1}{b} \\ \alpha \end{Bmatrix} \qquad \text{CONTROL LAW A}$$

$$\begin{Bmatrix} \beta \\ \delta \end{Bmatrix} = \begin{bmatrix} 0 & 0 \\ 2.7 & -5.3 \end{bmatrix} \begin{Bmatrix} \frac{h_1}{b} \\ \alpha \end{Bmatrix} + i \begin{bmatrix} 0 & 2.5\ (6.0) \\ 1.0\ (4.0) & .75\ (2.0) \end{bmatrix} \begin{Bmatrix} \frac{h_1}{b} \\ \alpha \end{Bmatrix} \qquad \text{CONTROL LAW B}$$

$$\begin{Bmatrix} \beta \\ \delta \end{Bmatrix} = \begin{bmatrix} 0 & 0 \\ 2.7 & -5.3 \end{bmatrix} \begin{Bmatrix} \frac{h_1}{b} \\ \alpha \end{Bmatrix} + i \begin{bmatrix} 0 & 0 \\ 2.5\ (4.0) & .75\ (2.0) \end{bmatrix} \begin{Bmatrix} \frac{h_1}{b} \\ \alpha \end{Bmatrix} \qquad \text{CONTROL LAW C}$$

Figure 4.- Delta-wing model control laws.

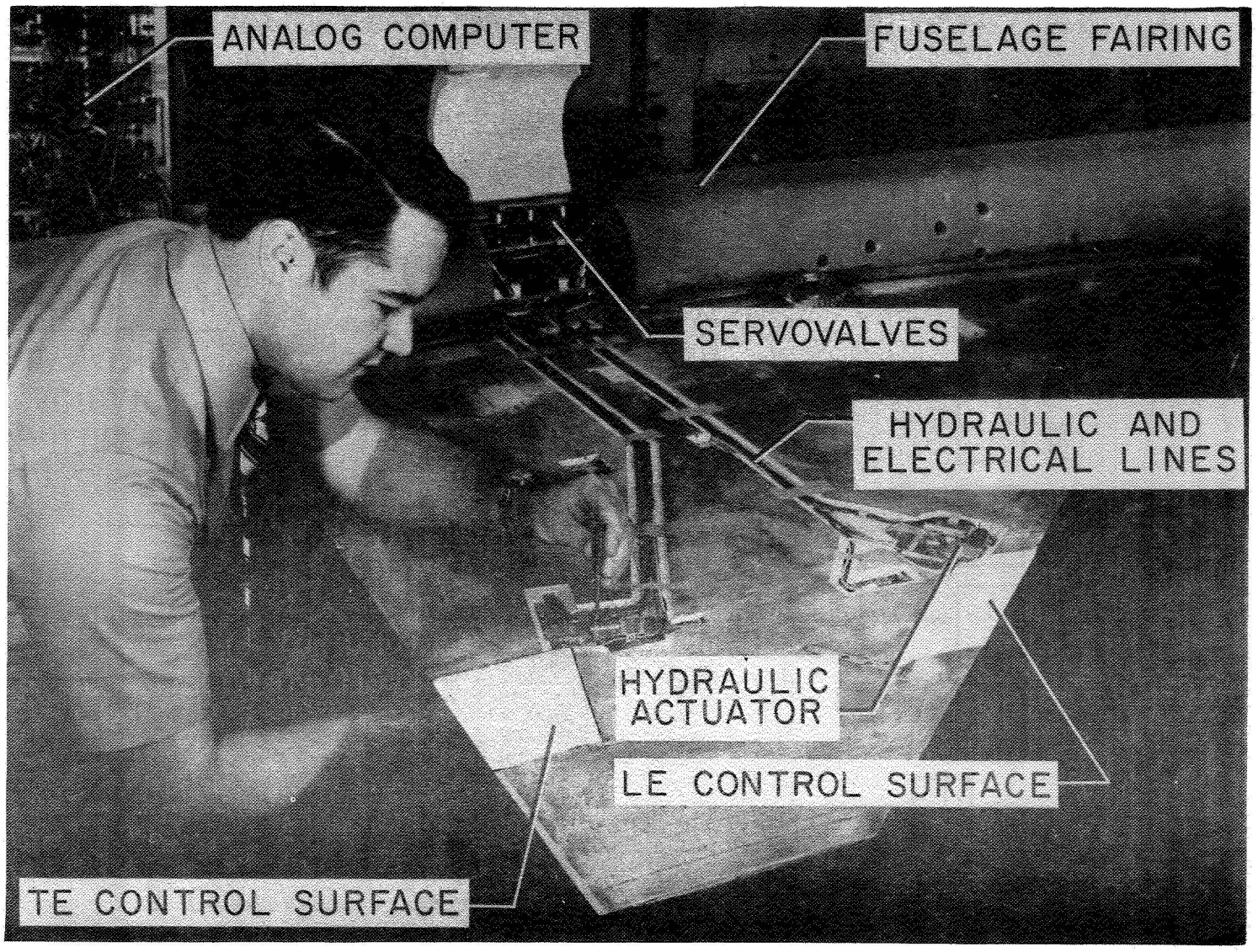

Figure 5.- Components of delta-wing flutter suppression system.

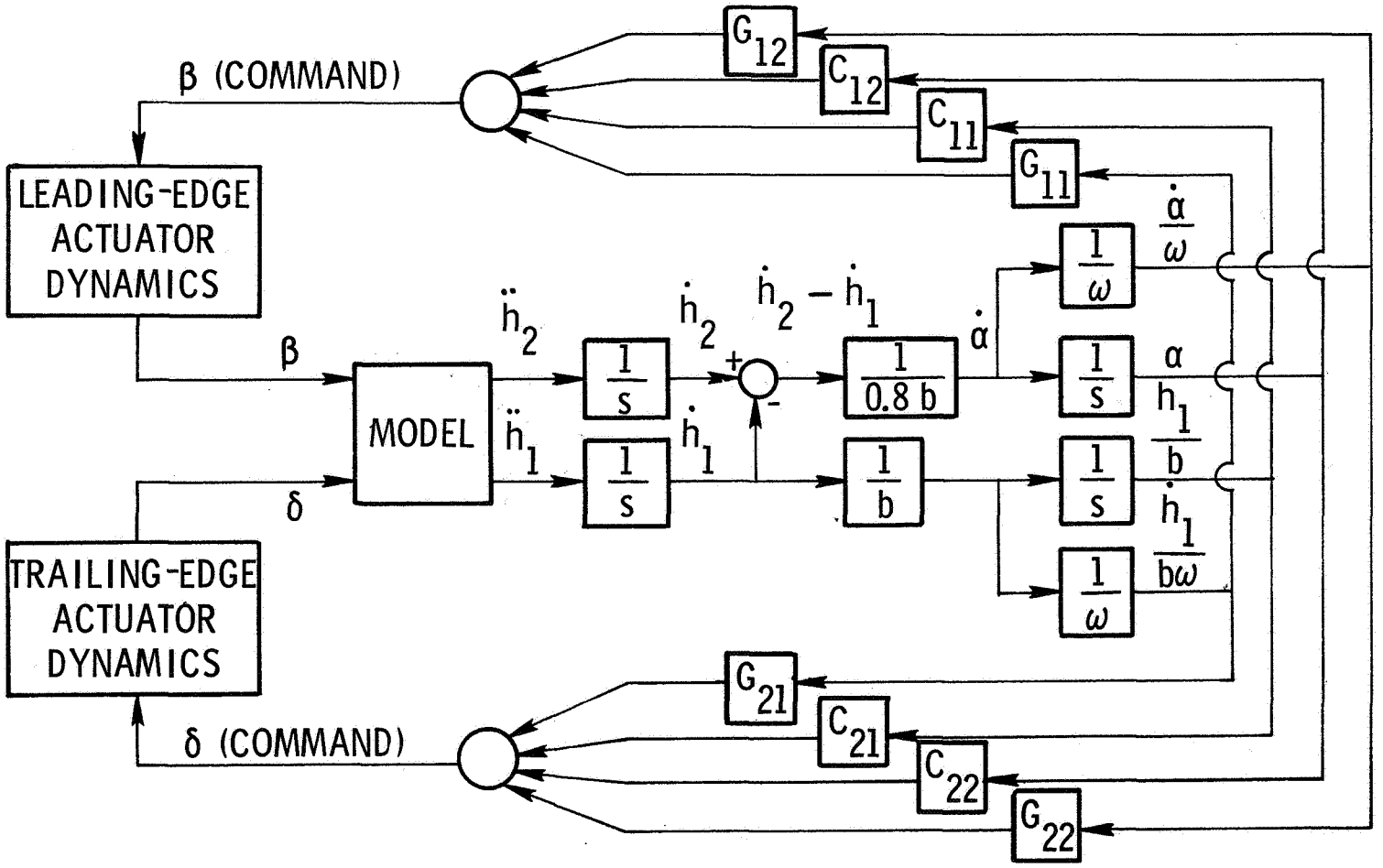

Figure 6.- Simplified block diagram of delta-wing flutter suppression system.

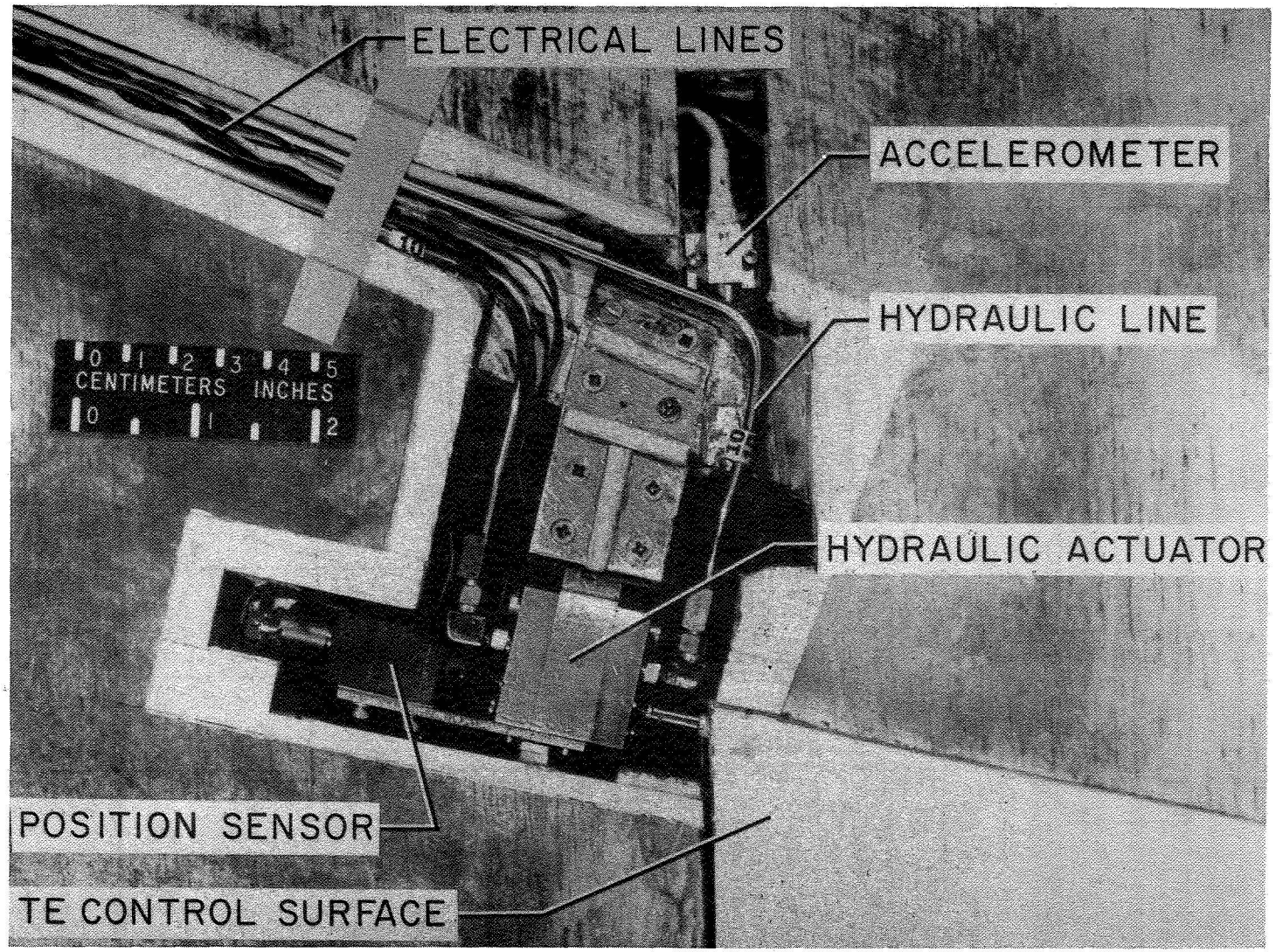

Figure 7.- Delta-wing trailing-edge control actuation system.

PERCENT INCREASE IN
FLUTTER DYNAMIC PRESSURE

SURFACE LOCATION	ACCELEROMETER LOCATION		
	INBOARD EDGE	CENTER LINE	OUTBOARD EDGE
INBOARD STRIP	18	22	21
MIDSPAN STRIP	26	17	8
OUTBOARD STRIP	6	25	36

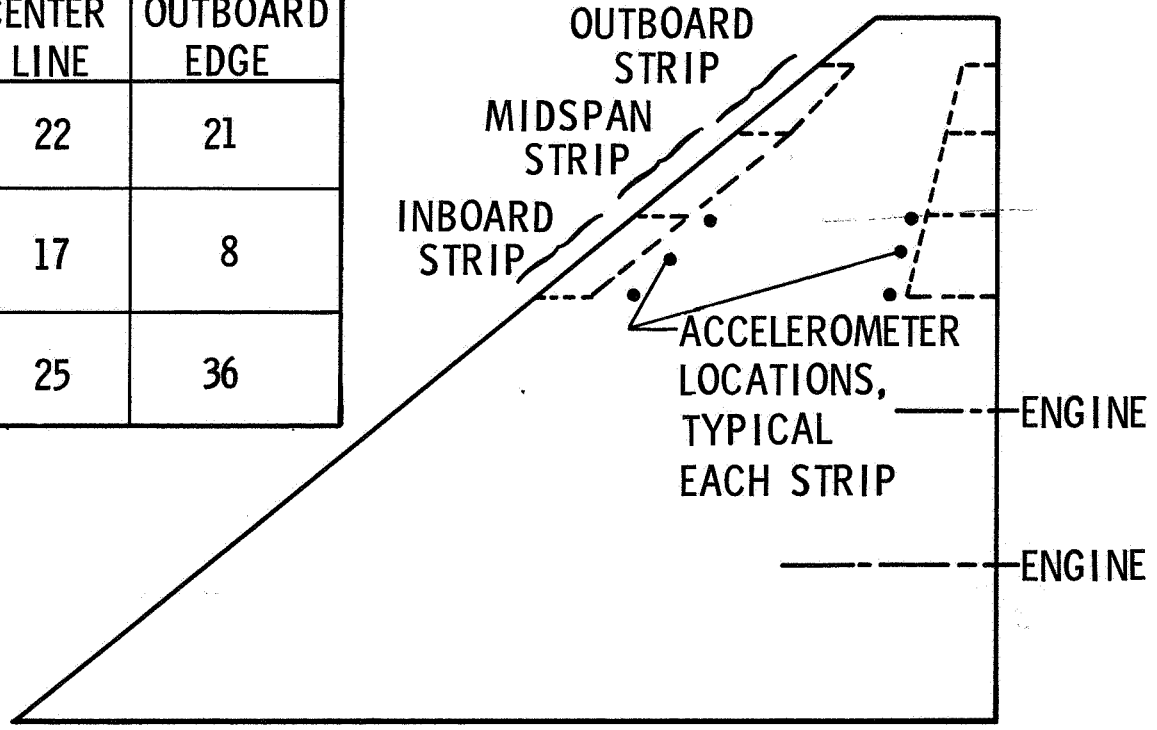

Figure 8.- Effects of control surface and accelerometer locations on flutter dynamic pressure.

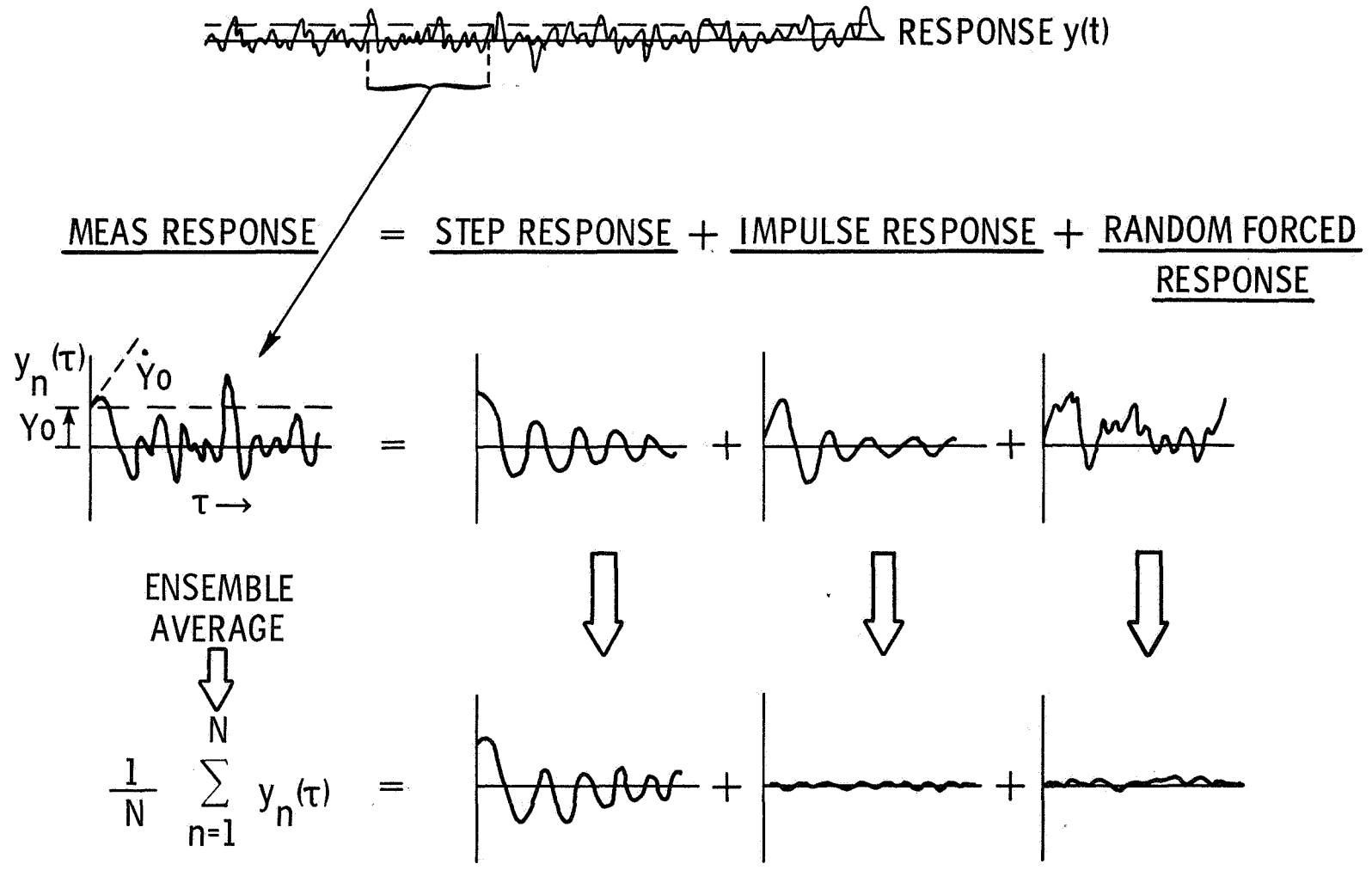

Figure 9.- Basic randomdec concepts.

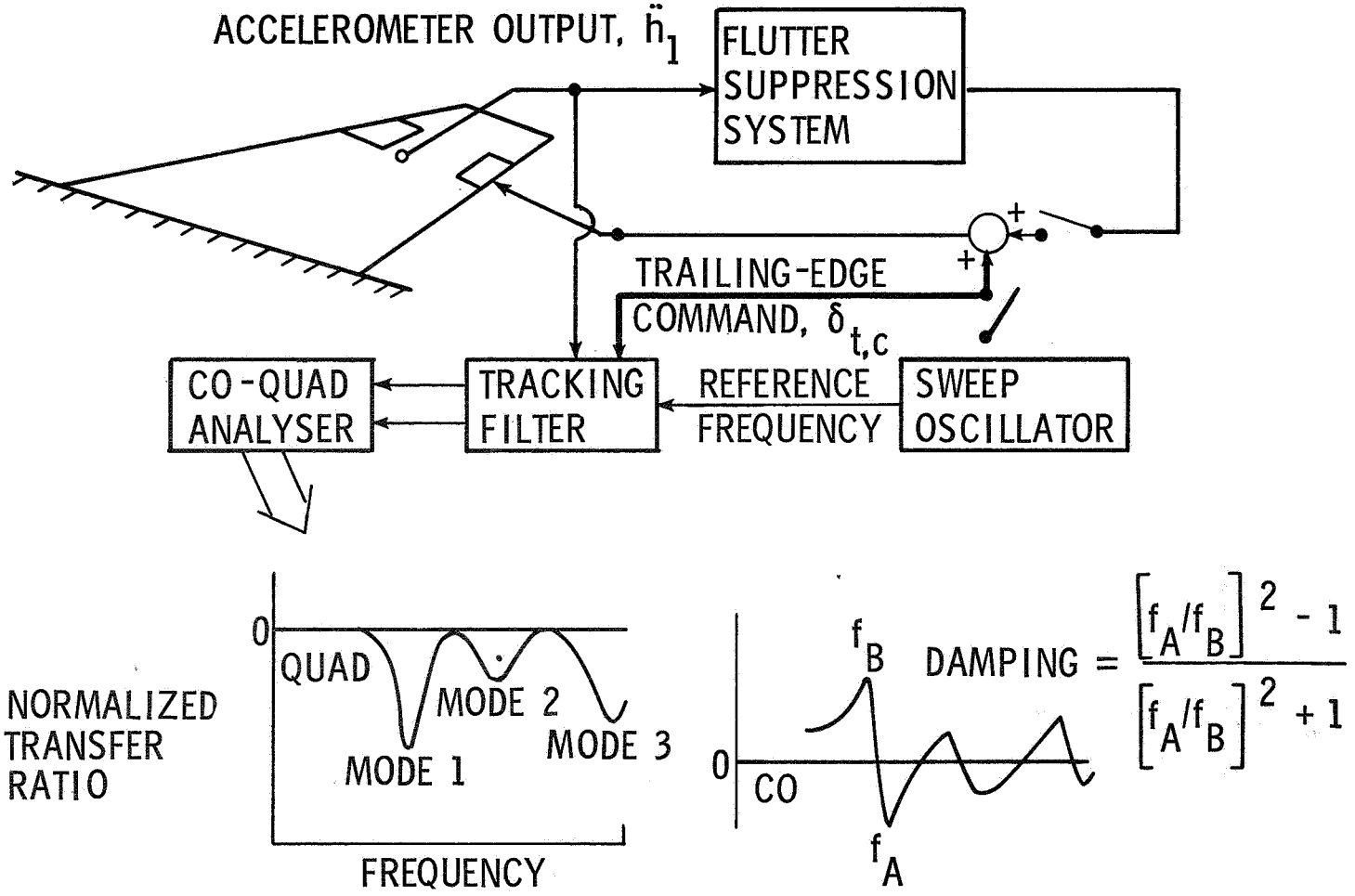

Figure 10.- Co-Quad subcritical response method.

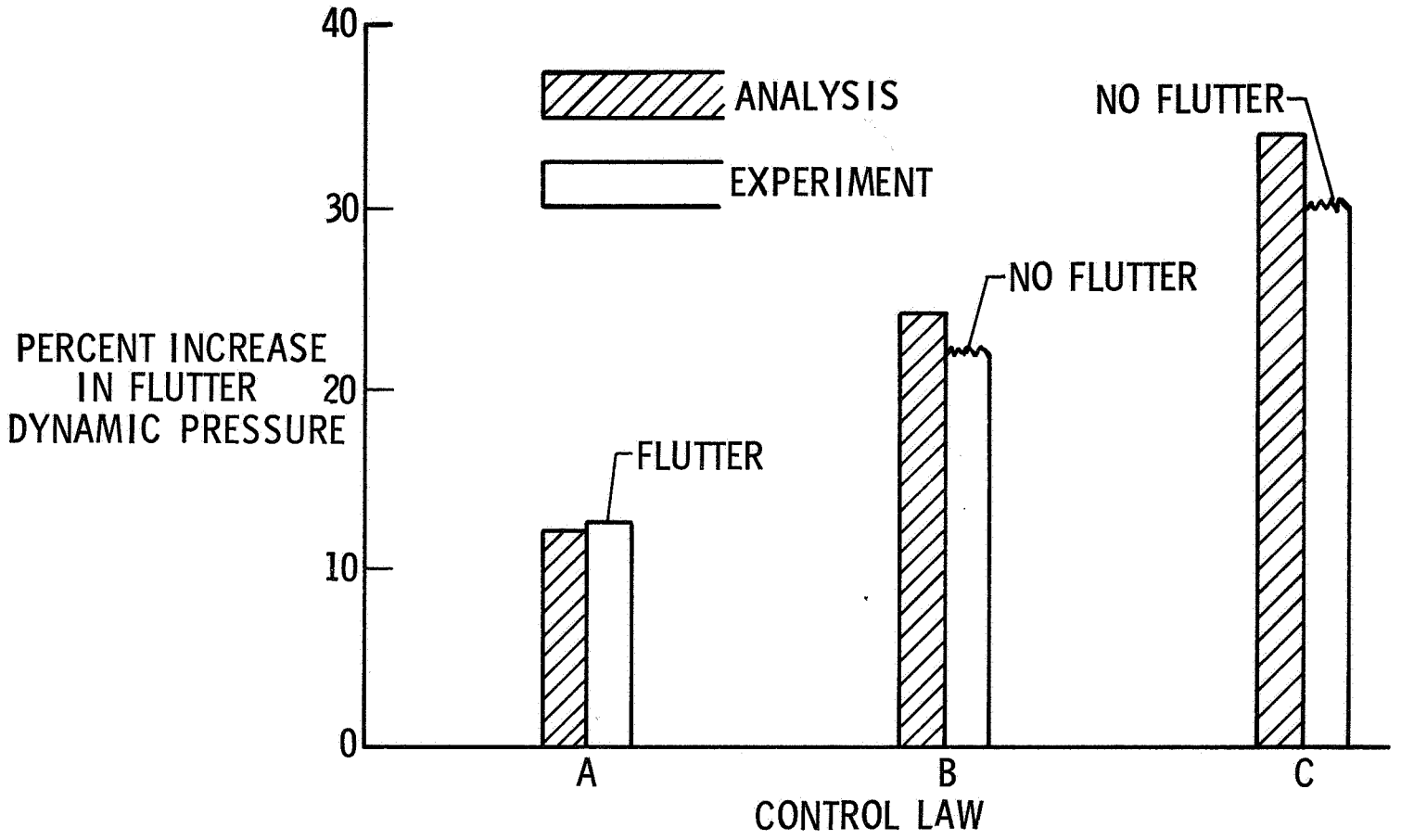

Figure 11.- Effect of different control laws on flutter dynamic pressure at M = 0.9.

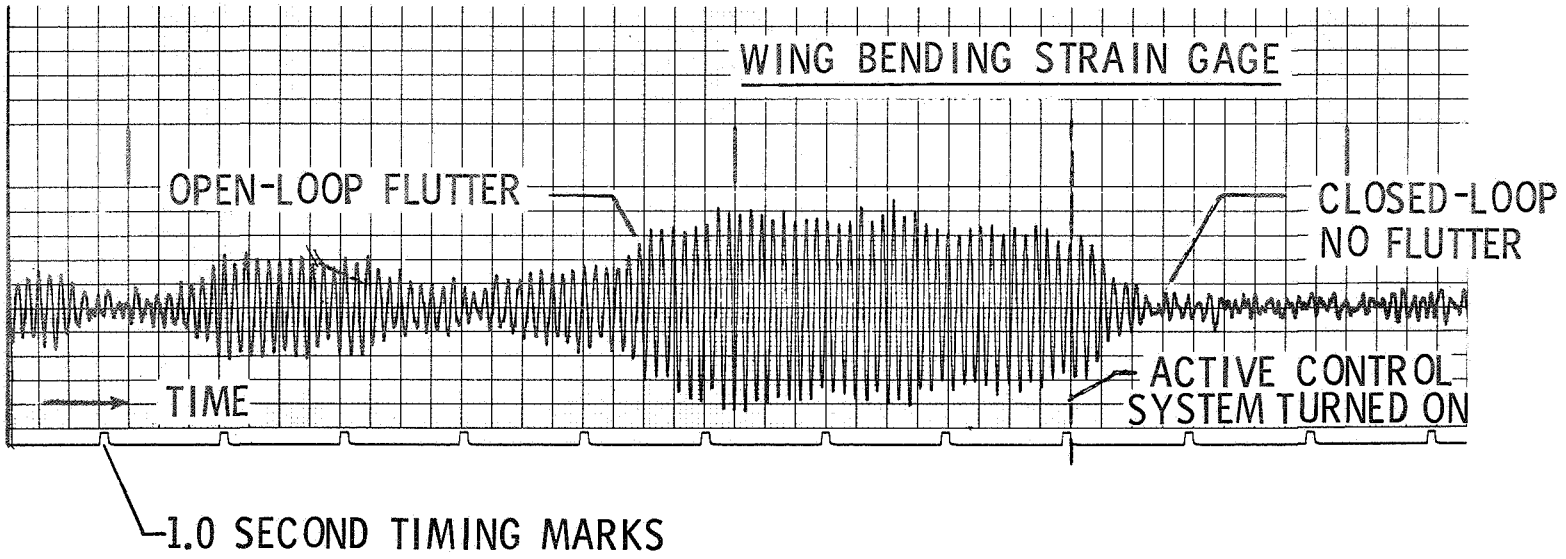

Figure 12.- Time history trace showing effective operation of delta-wing flutter suppression system (Control Law C).

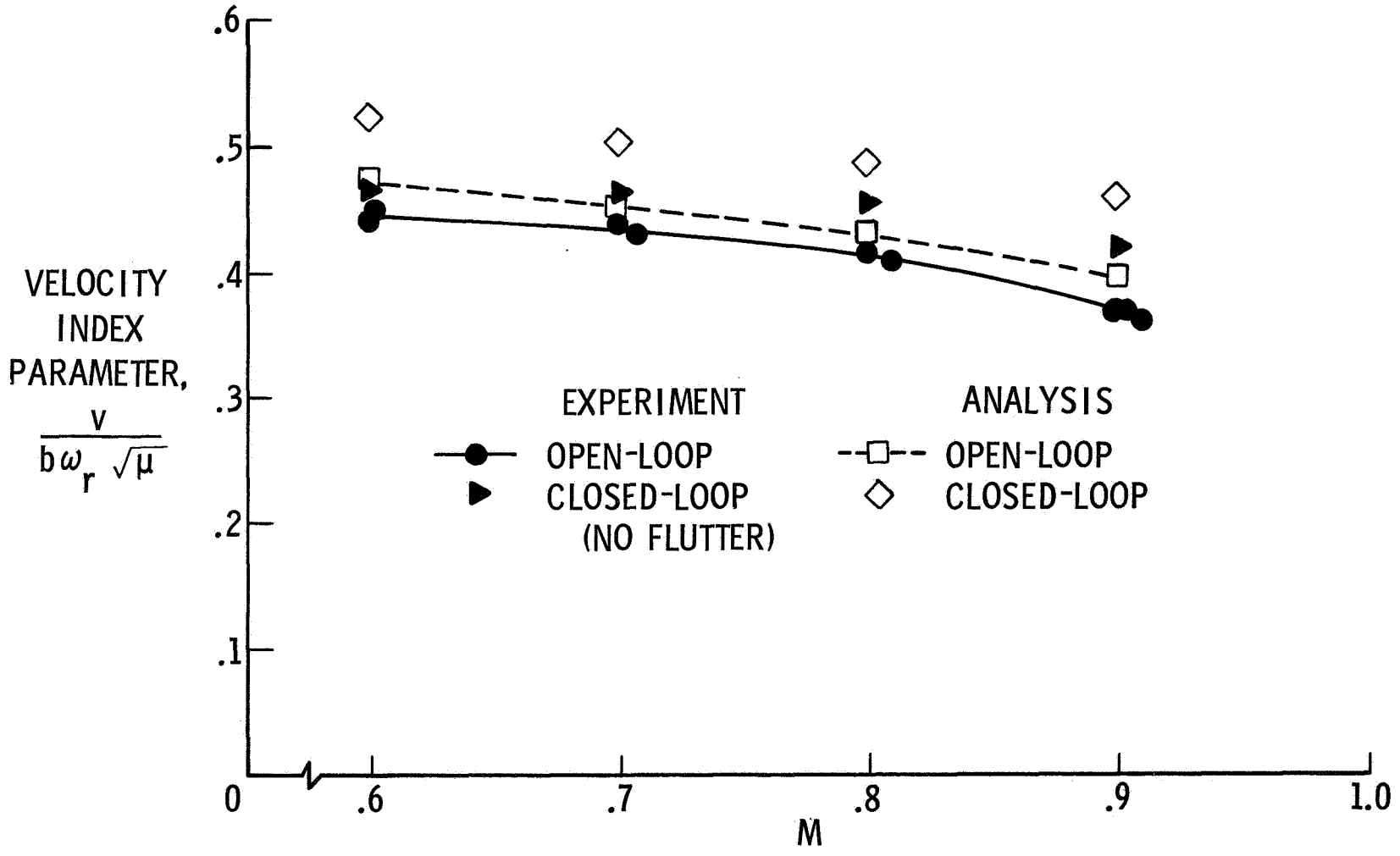

Figure 13.- Measured and calculated variation of flutter velocity index parameter with Mach number.

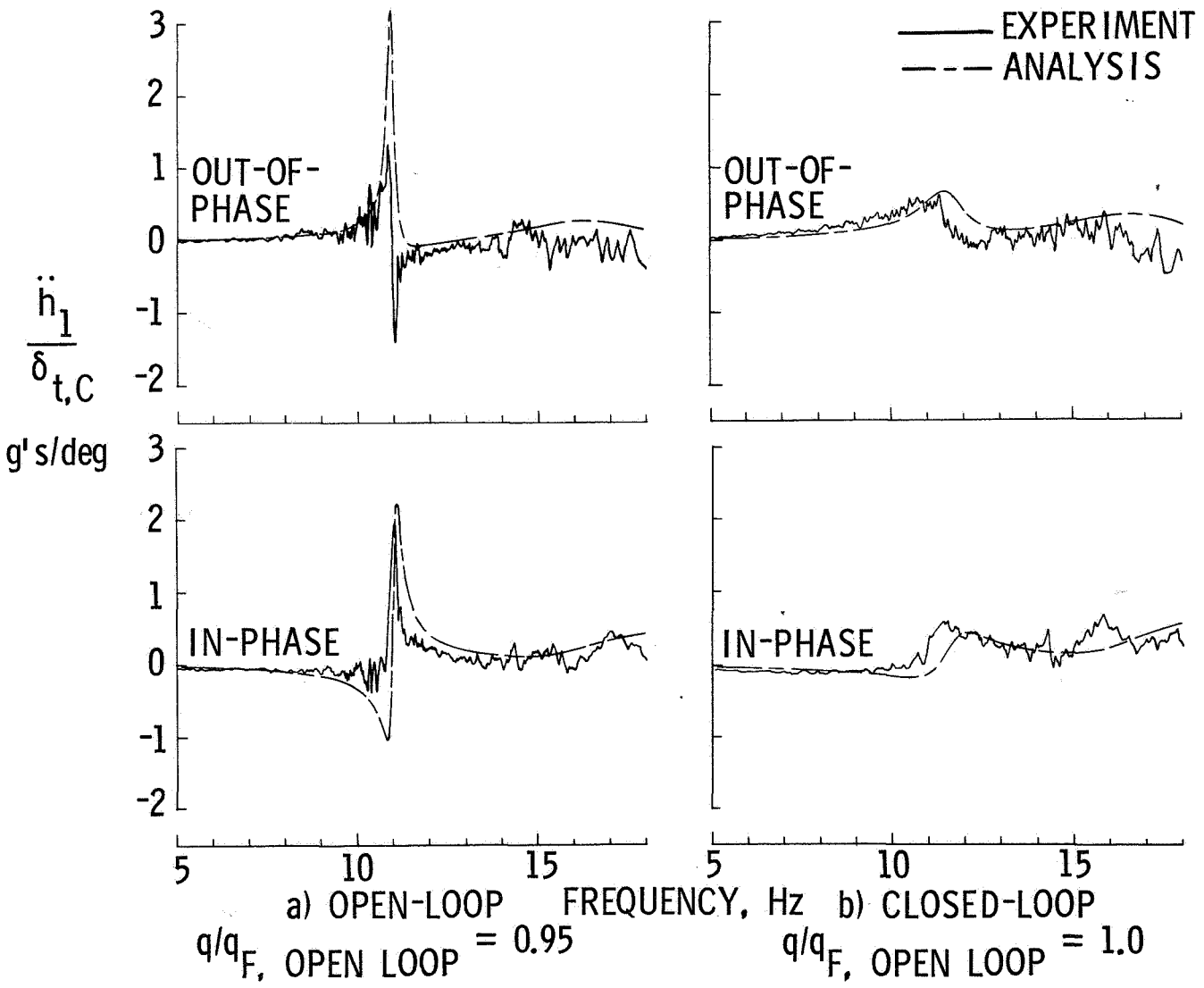

Figure 14.- A comparison of measured and calculated forced response to trailing-edge-control excitation at M = 0.9.

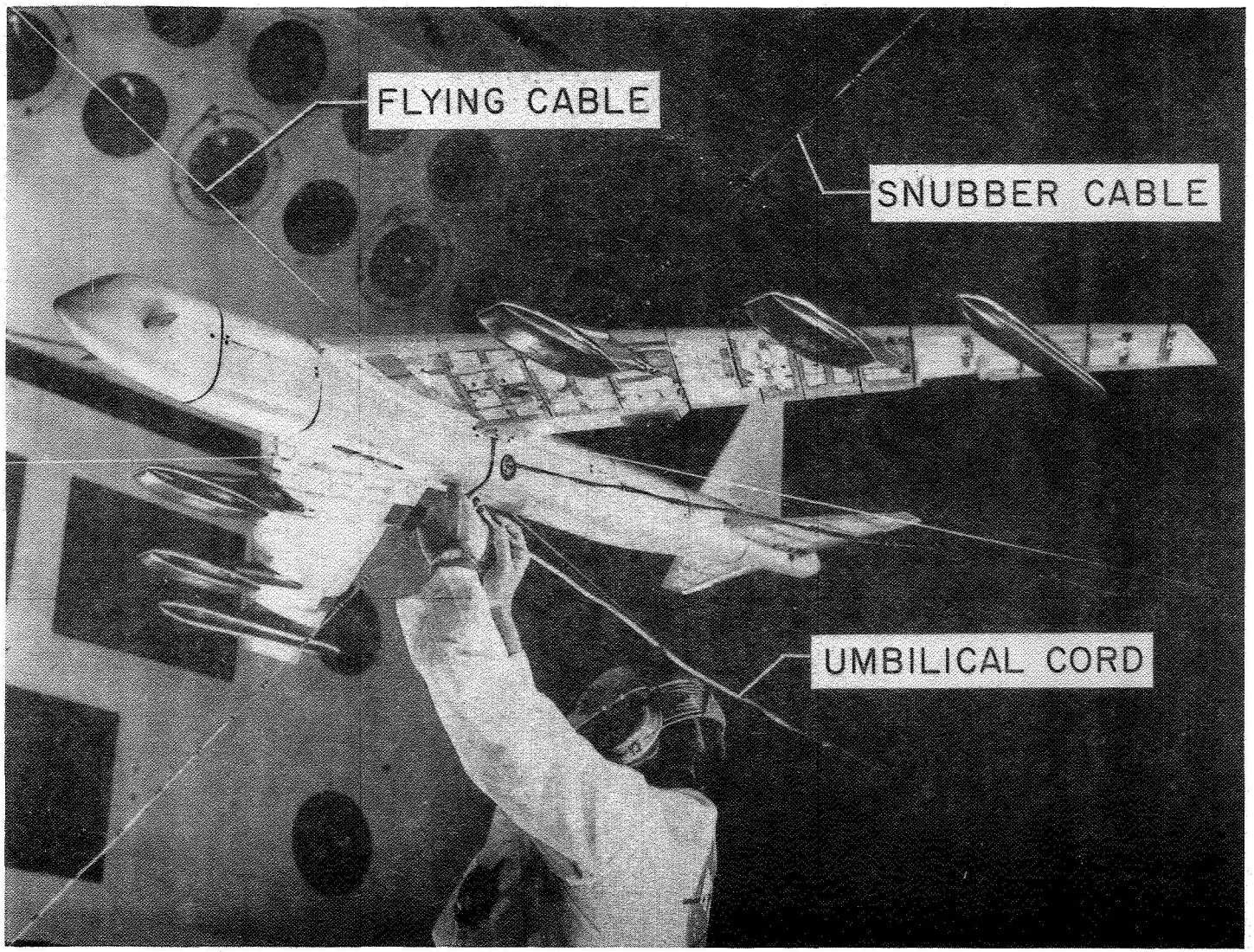

Figure 15. B-52 model mounted in transonic dynamics tunnel.

Figure 16.- B-52 model control surface and sensor locations.

- FROUDE NUMBER, $\frac{\text{FLUID ACCELERATION}}{\text{GRAVITY ACCELERATION}}$, $\frac{V^2}{Lg}$
- REDUCED WAVELENGTH, $\frac{\text{FLUID VELOCITY}}{\text{VIBRATION VELOCITY}}$, $\frac{V}{\omega L}$
- MASS RATIO, $\frac{\text{MASS OF BODY}}{\text{APPARENT MASS OF FLUID}}$, $\frac{m}{\rho_f L^3}$

MODEL / AIRPLANE DESIGN CONDITIONS

	AIRPLANE	MODEL
GROSS WEIGHT	170 097 Kgm	25.67 Kgm
ALTITUDE	6 400 m (FMC) 1 646 m (RQC)	———
DENSITY	.631 Kg/m^3 (FMC) 1.041 Kg/m^3 (RQC)	2.572 Kg/m^3 4.123 Kg/m^3
MEDIUM	AIR	FREON (95%)

Figure 17.- B-52 model scaling parameters.

Figure 18.- Exposed view of B-52 model.

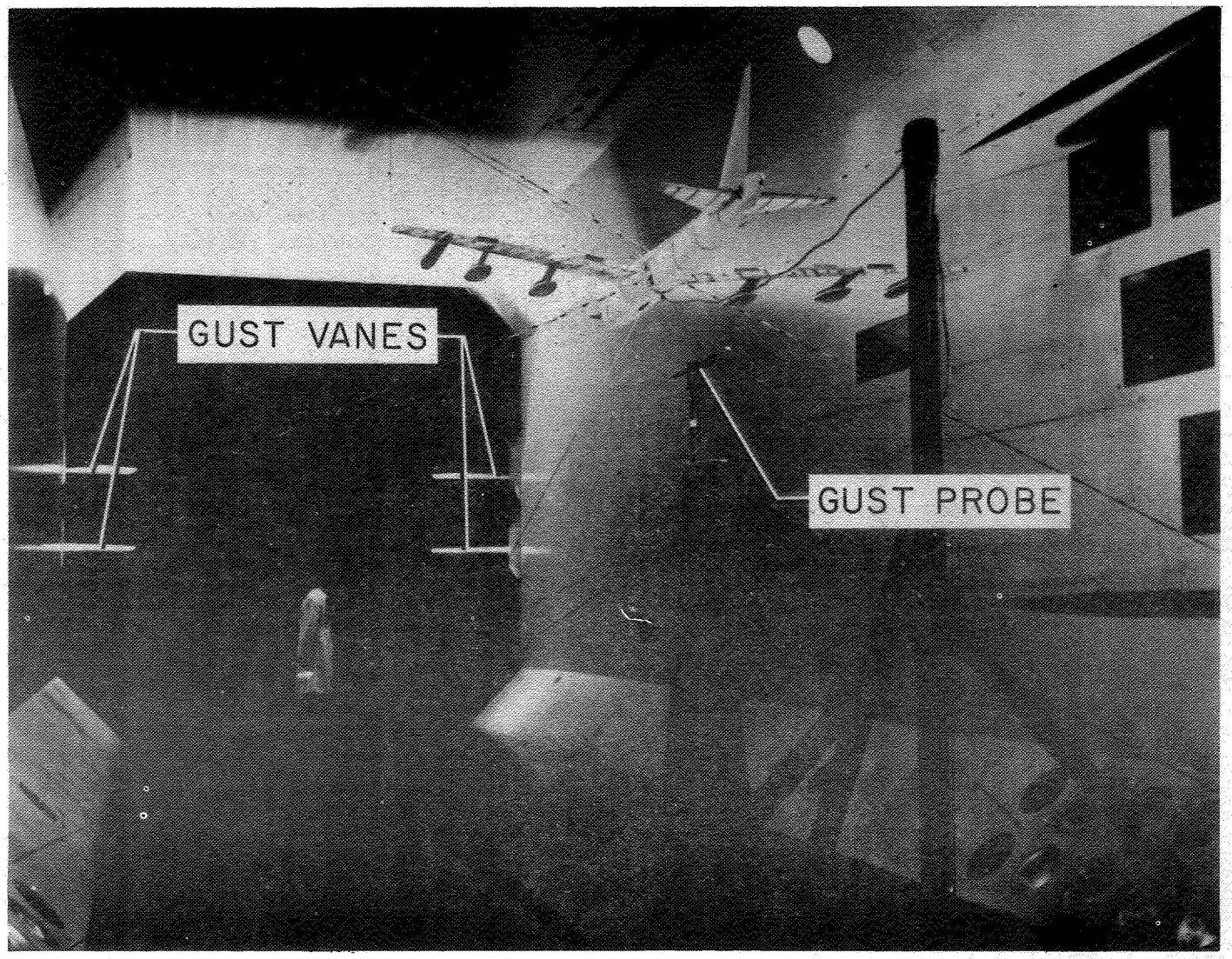

Figure 19.- View of B-52 model showing gust generating vanes.

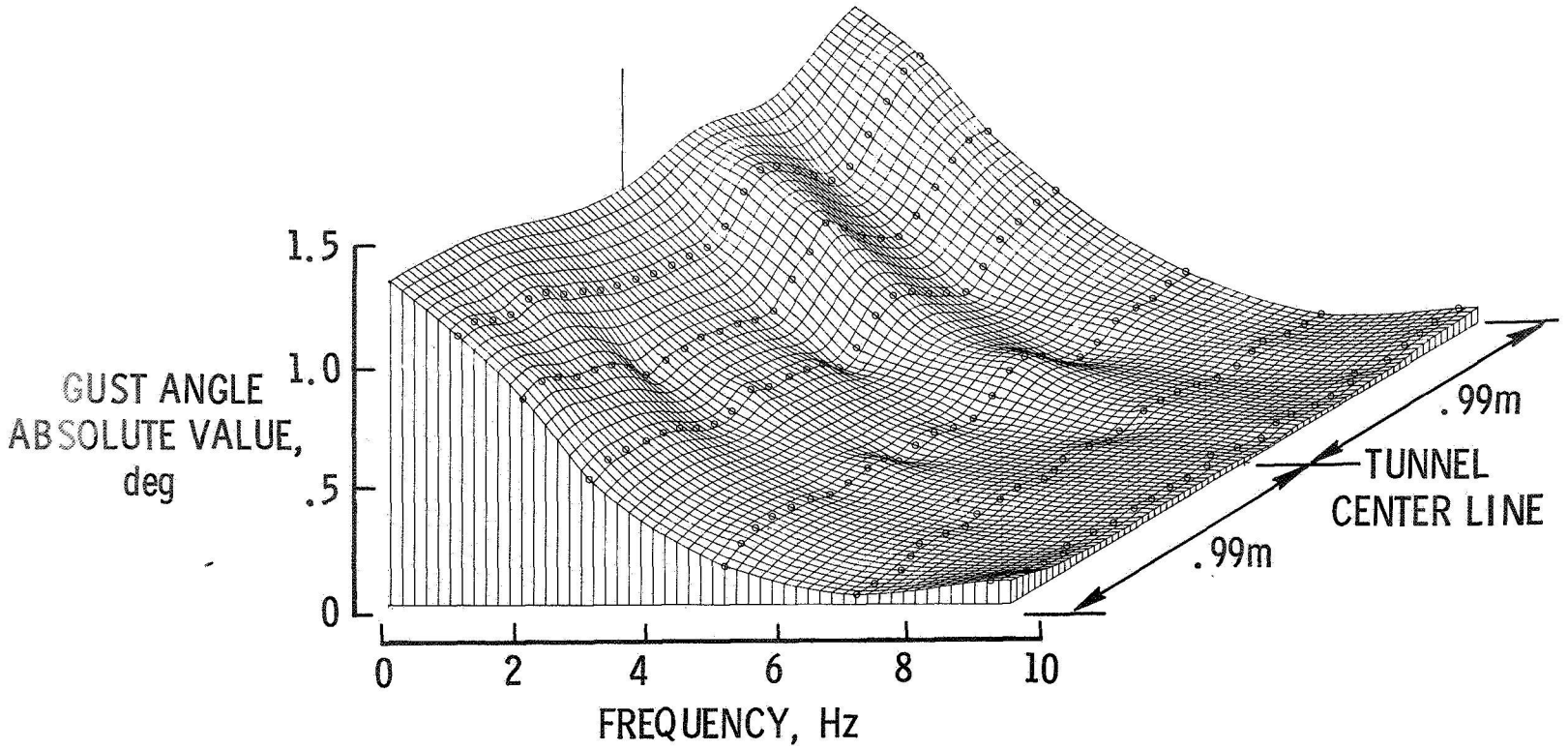

Figure 20.- Typical variation of gust flow angle with frequency and tunnel lateral position for an oscillating vane angle of 6° and a velocity of 35.4 m/sec.

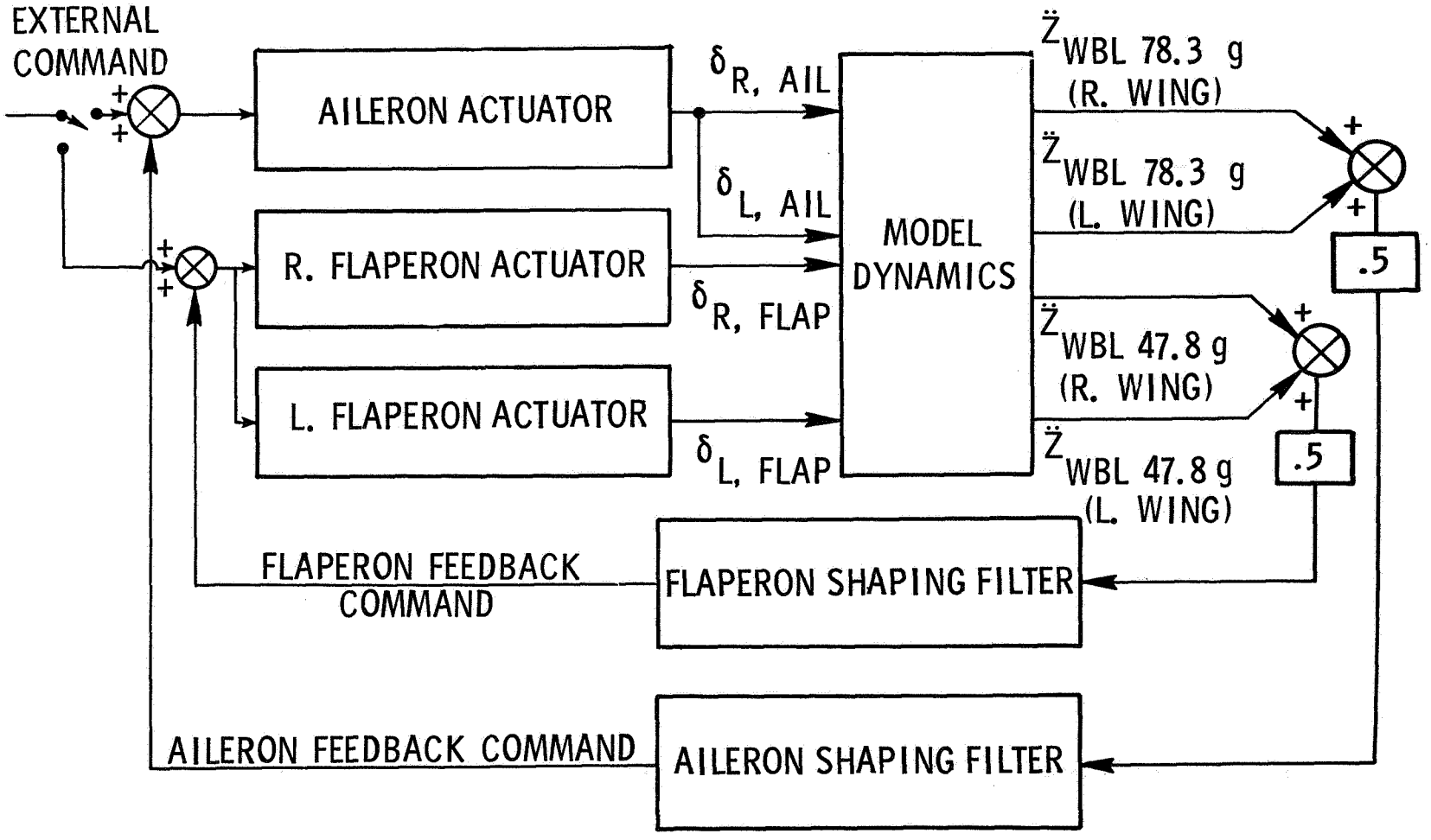

Figure 21.- Simplified block diagram of B-52 model FMC system.

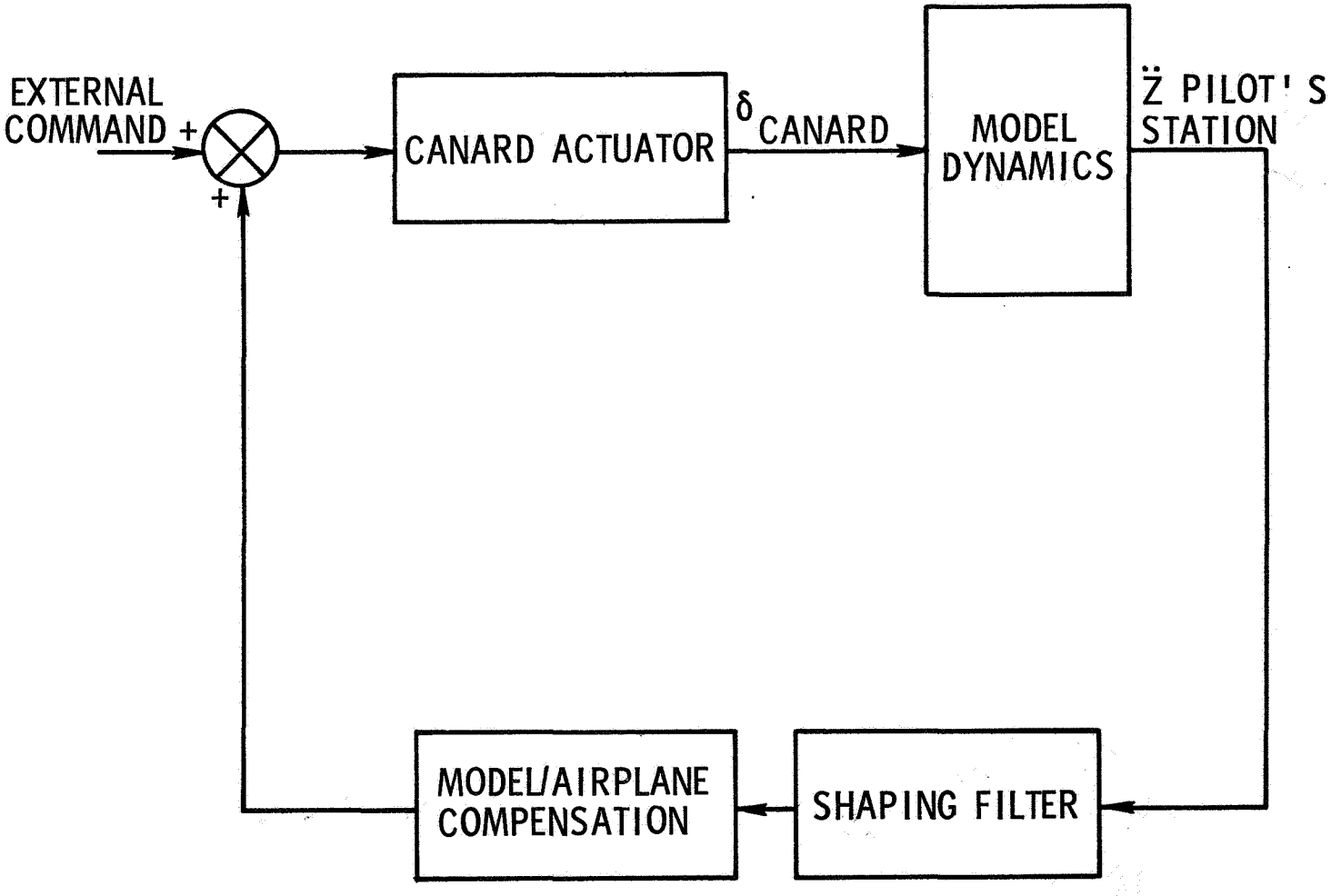

Figure 22.- Simplified block diagram of B-52 model RQC system.

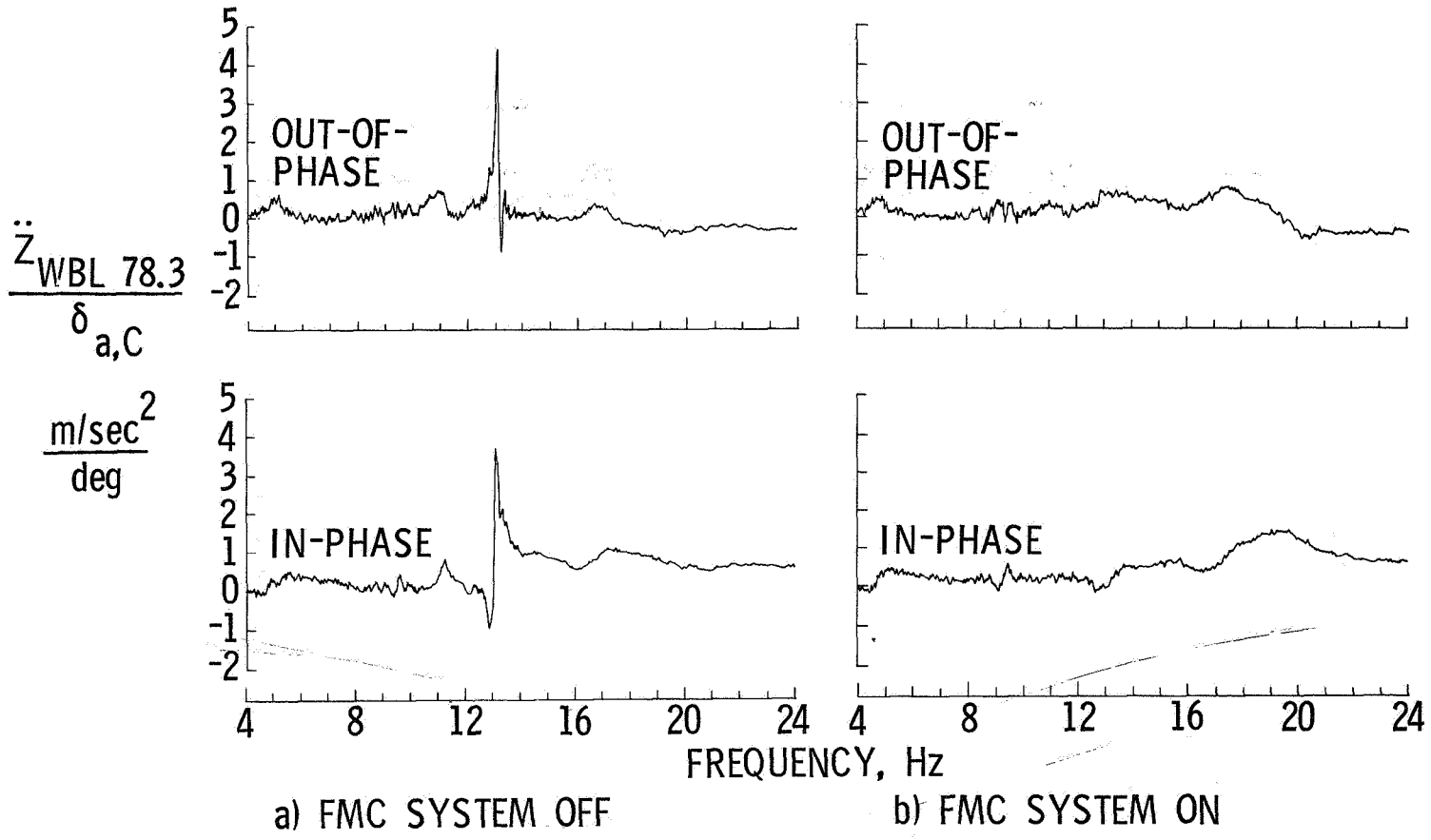

Figure 23.- Measured frequency response of B-52 model to aileron excitation at a velocity 6 percent below open-loop flutter velocity.

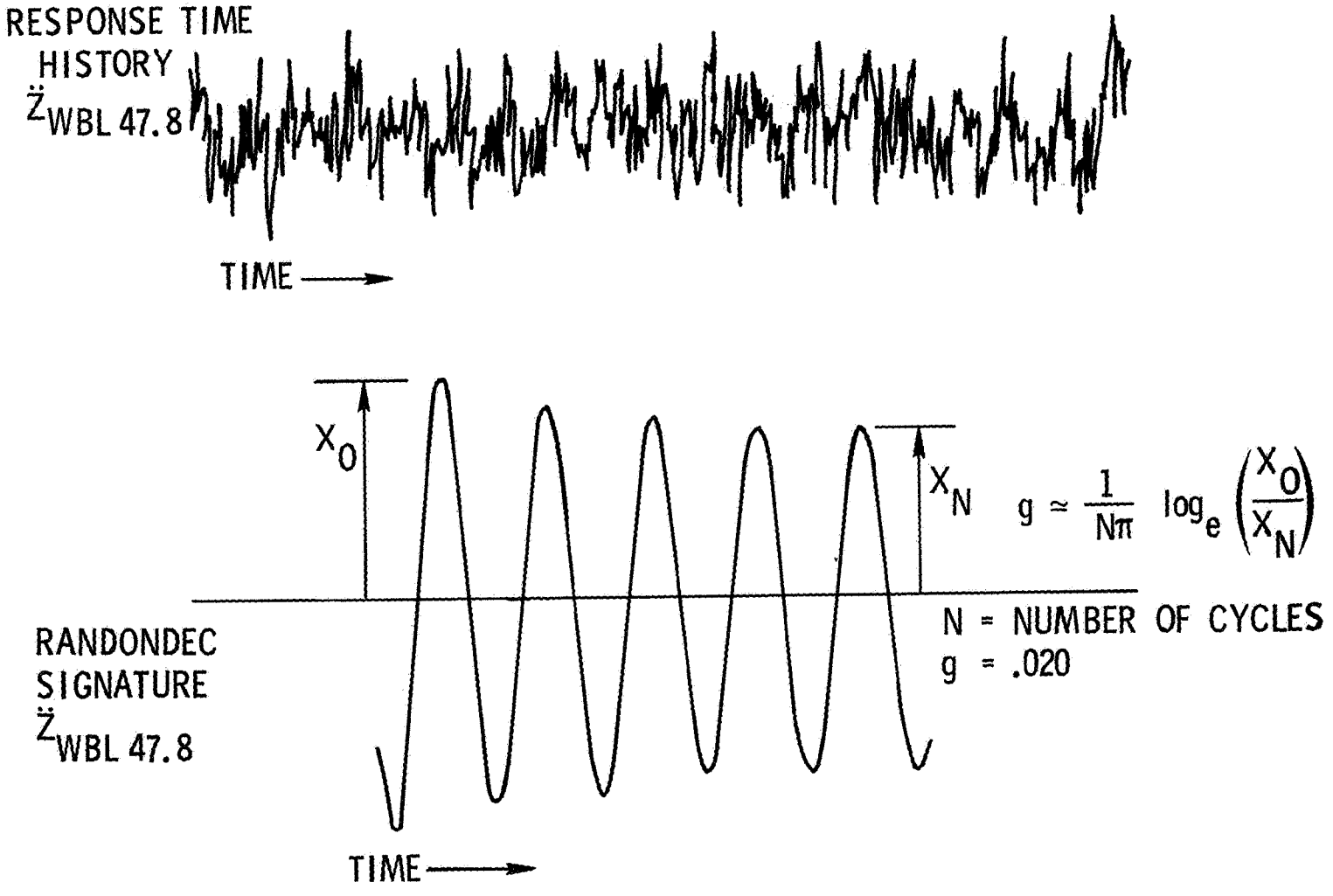

Figure 24.- Wing response as measured with randomdec technique at a velocity of 3 percent below open-loop flutter velocity.

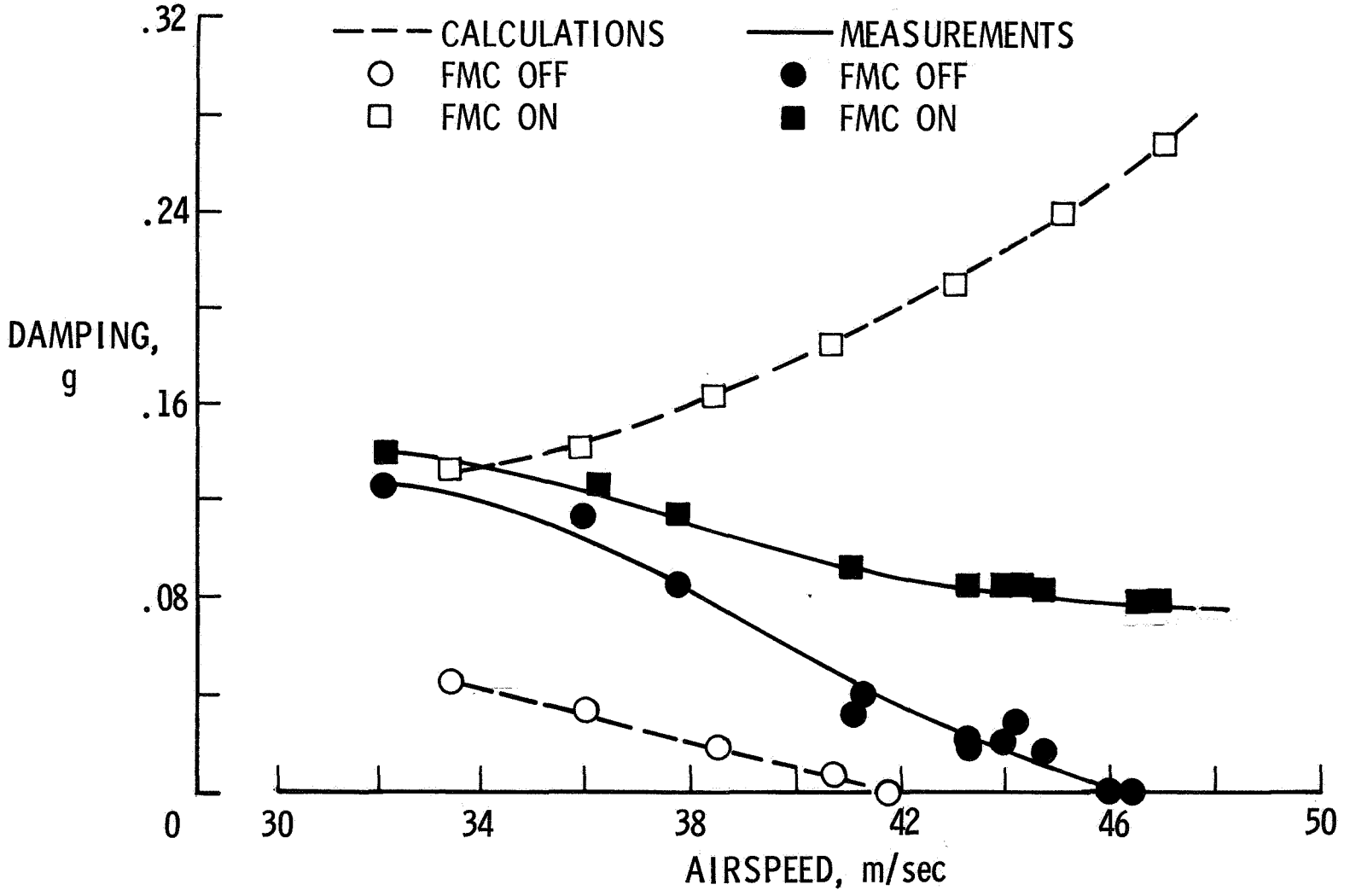

Figure 25.- Comparison of measured and calculated damping for the B-52 model.

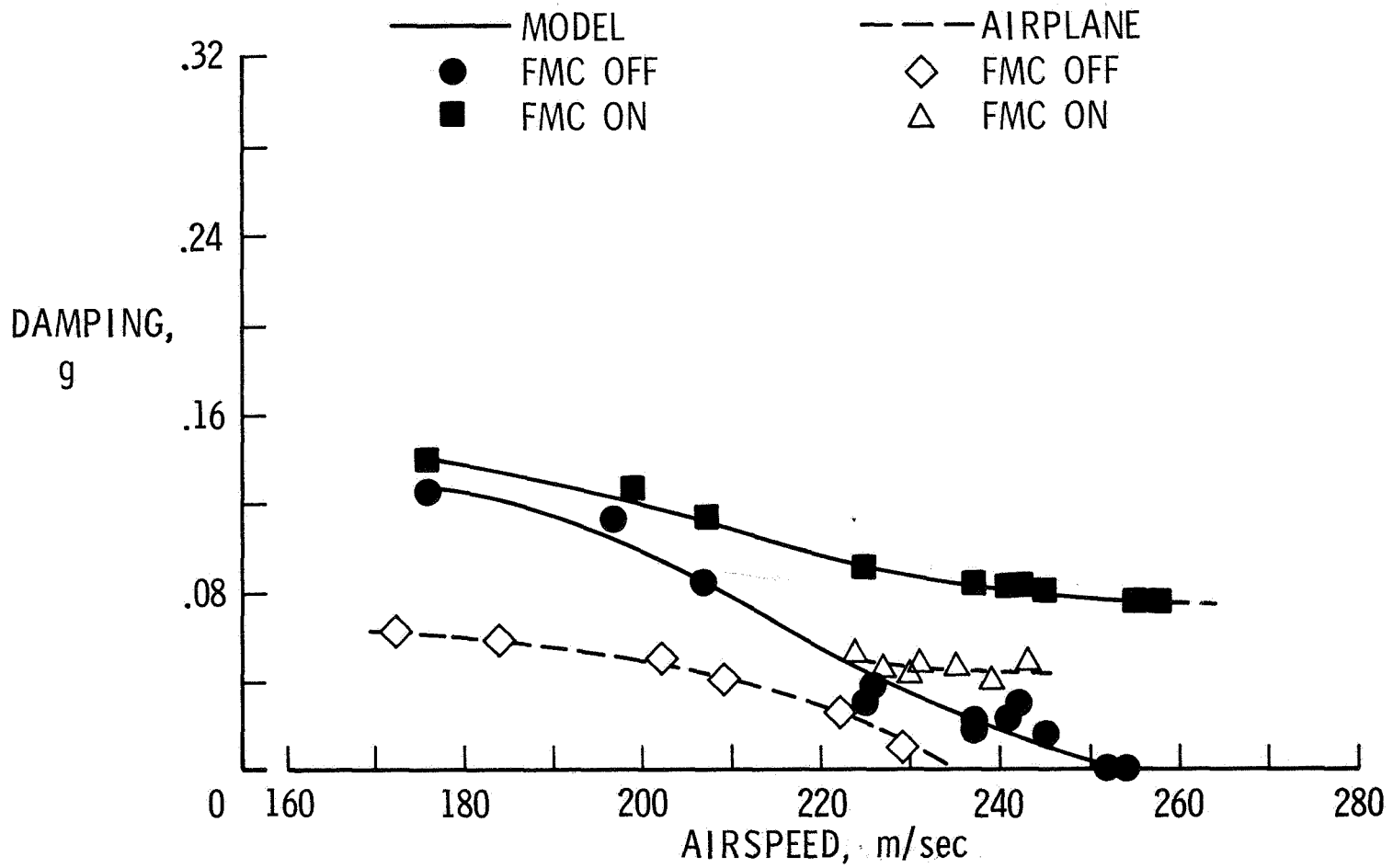

Figure 26.- Comparison of B-52 CCV model and airplane damping characteristics of the flutter mode.

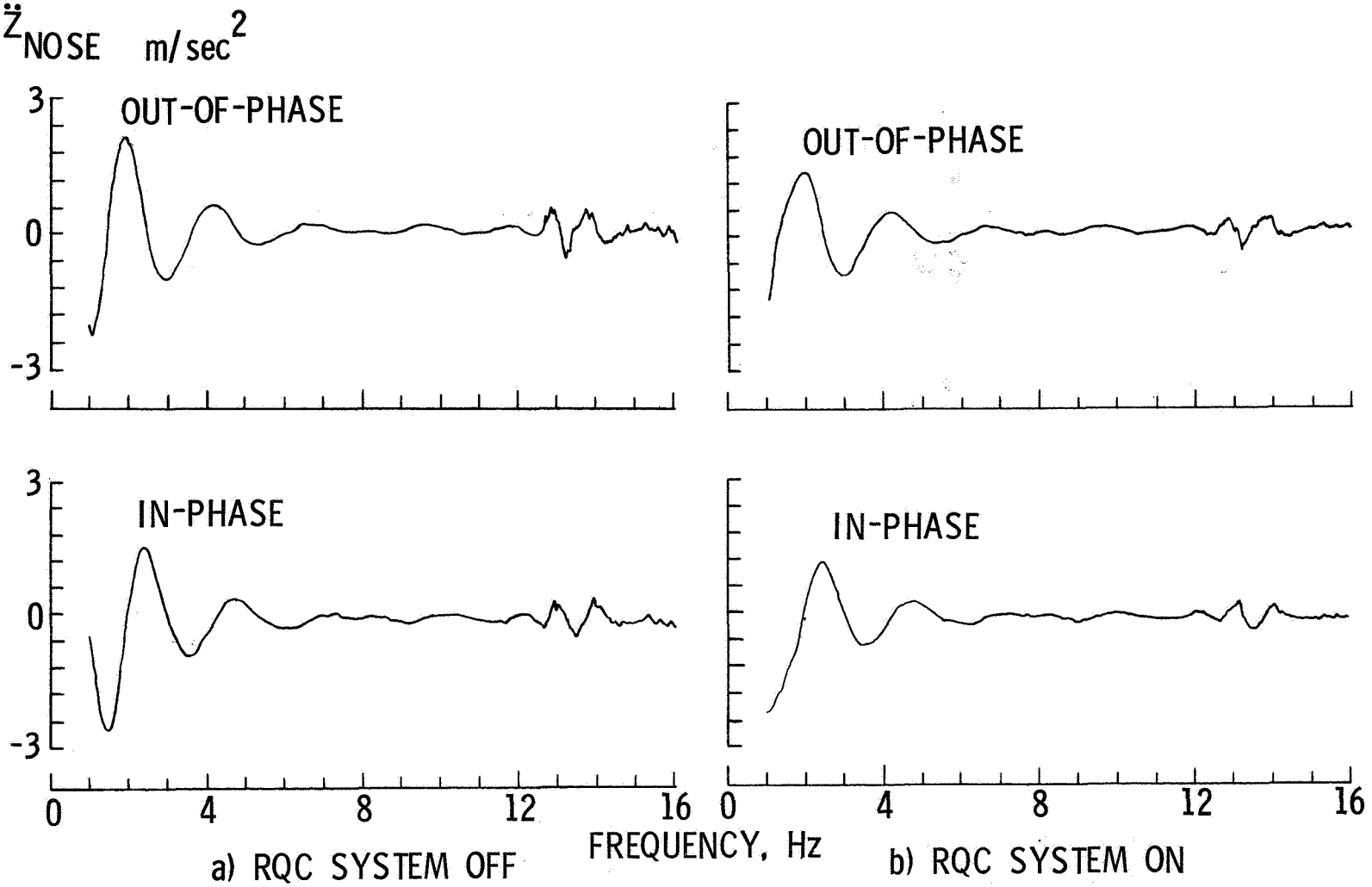

Figure 27.- Measured frequency response of B-52 model to oscillating gust vane excitation for a vane angle of 6° and a velocity of 33.7 m/sec.

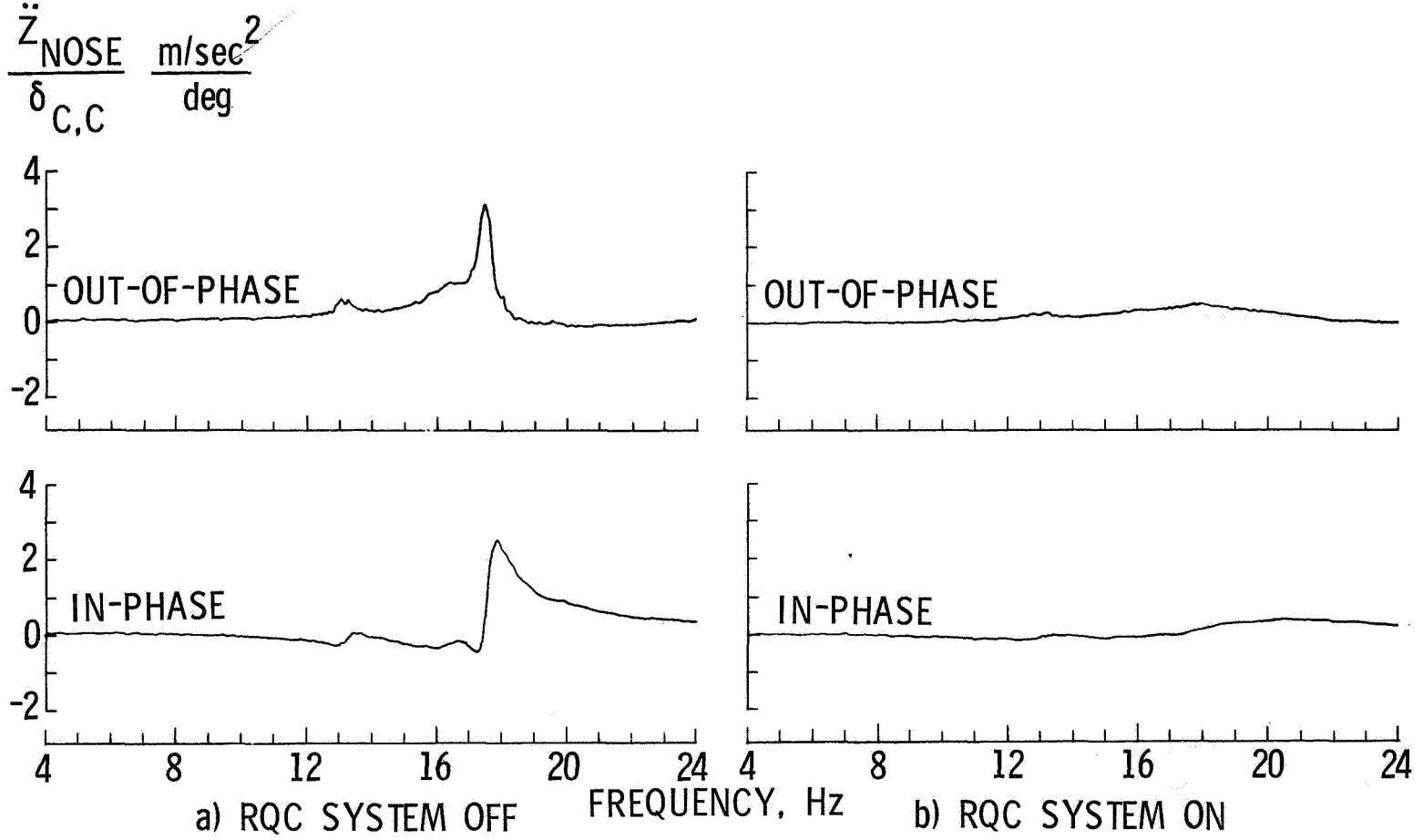

Figure 28.- Measured frequency response of B-52 model to canard excitation at a velocity of 33.7 m/sec.

Figure 29.- C-5A model mounted in transonic dynamics tunnel.

Figure 30.- Exposed view of rear portion of C-5A model fuselage.

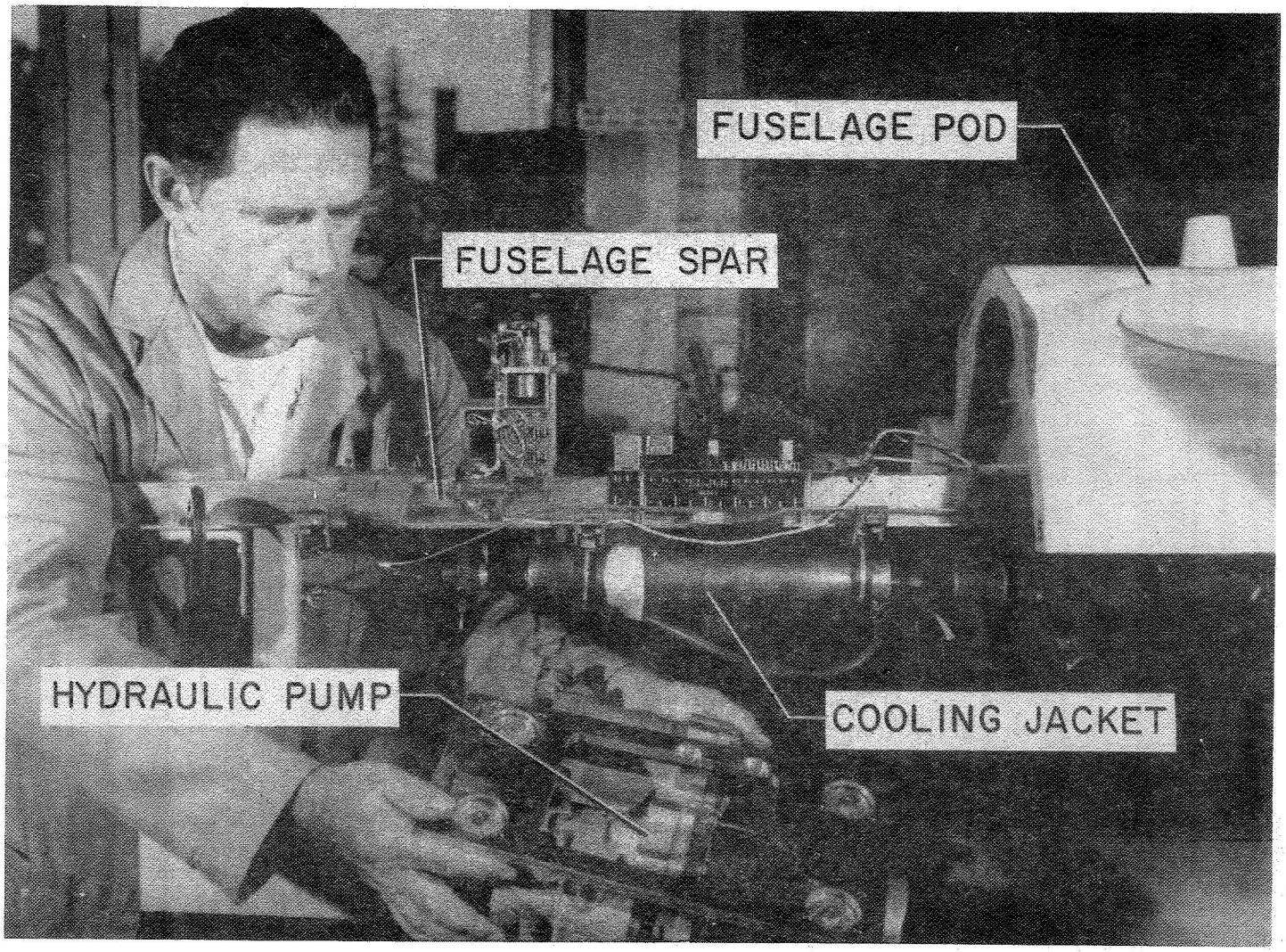

Figure 31.- Exposed view of forward portion of C-5A model fuselage.

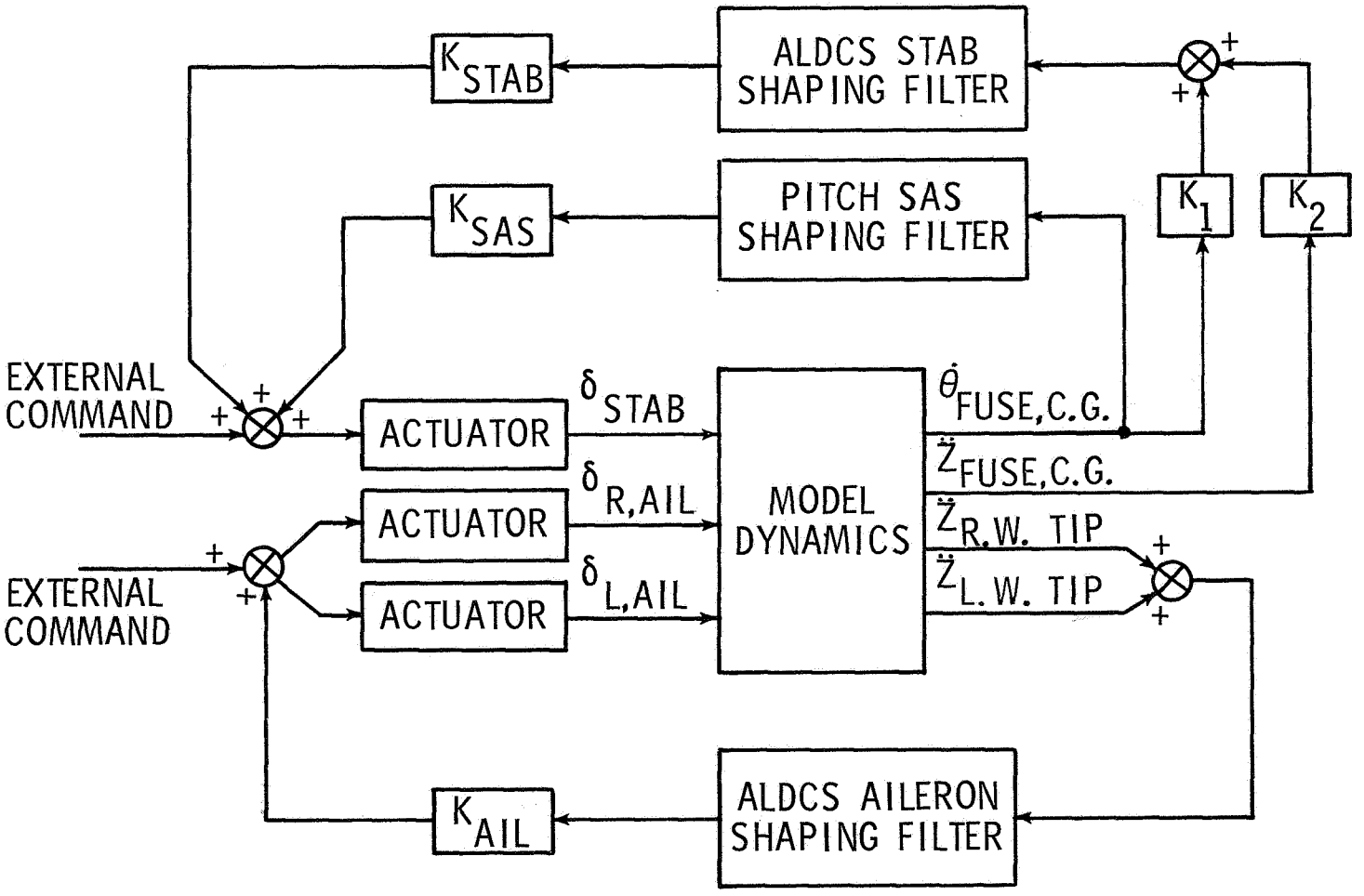

Figure 32.- Simplified block diagram of C-5A active lift distribution control system (ALDCS).

PURPOSE	FIXED TEST CONDITIONS	PRIMARY TEST VARIABLE	OTHER TEST VARIABLES
MODEL TEST CONFIGURATION: 33-PERCENT WING FUEL			
STATIC AERODYNAMICS	MODEL FREE-FLYING LIFT DEVICE USED ALDCS OFF	ANGLE OF ATTACK	AILERON UPRIG
DYNAMIC LOADS	MODEL SNUBBED AND RESTRAINED ALDCS OFF AILERON UPRIG $+5^{0}$	AILERON AND STABILIZER FREQUENCY SWEEP	AILERON SWEEP AMPLITUDE STABILIZER SWEEP AMPLITUDE
MODEL TEST CONFIGURATIONS: 0-PERCENT AND 33-PERCENT WING FUEL			
ALDCS EFFECTIVENESS	MODEL FREE-FLYING AILERON UPRIG +5°	ALDCS OFF/ON	AILERON SWEEP AMP. AILERON STEP/RAMPS STAB. SWEEP AMP. STAB. STEP/RAMPS SYM. GUST SWEEP ANTISYM. GUST SWEEP INCREASE ALDCS AILERON GAIN UNSTABLE CONTROL LAW PITCH SAS OFF/ON
ALDCS EFFECT ON FLUTTER	MODEL SNUBBED MODEL FREE-FLYING AILERON UPRIG $+5^{0}$	ALDCS OFF/ON	DYNAMIC PRESSURE MACH NUMBER AILERON STEP AILERON UPRIG $+8^{0}$

Figure 33.- C-5A ALDCS model test summary.

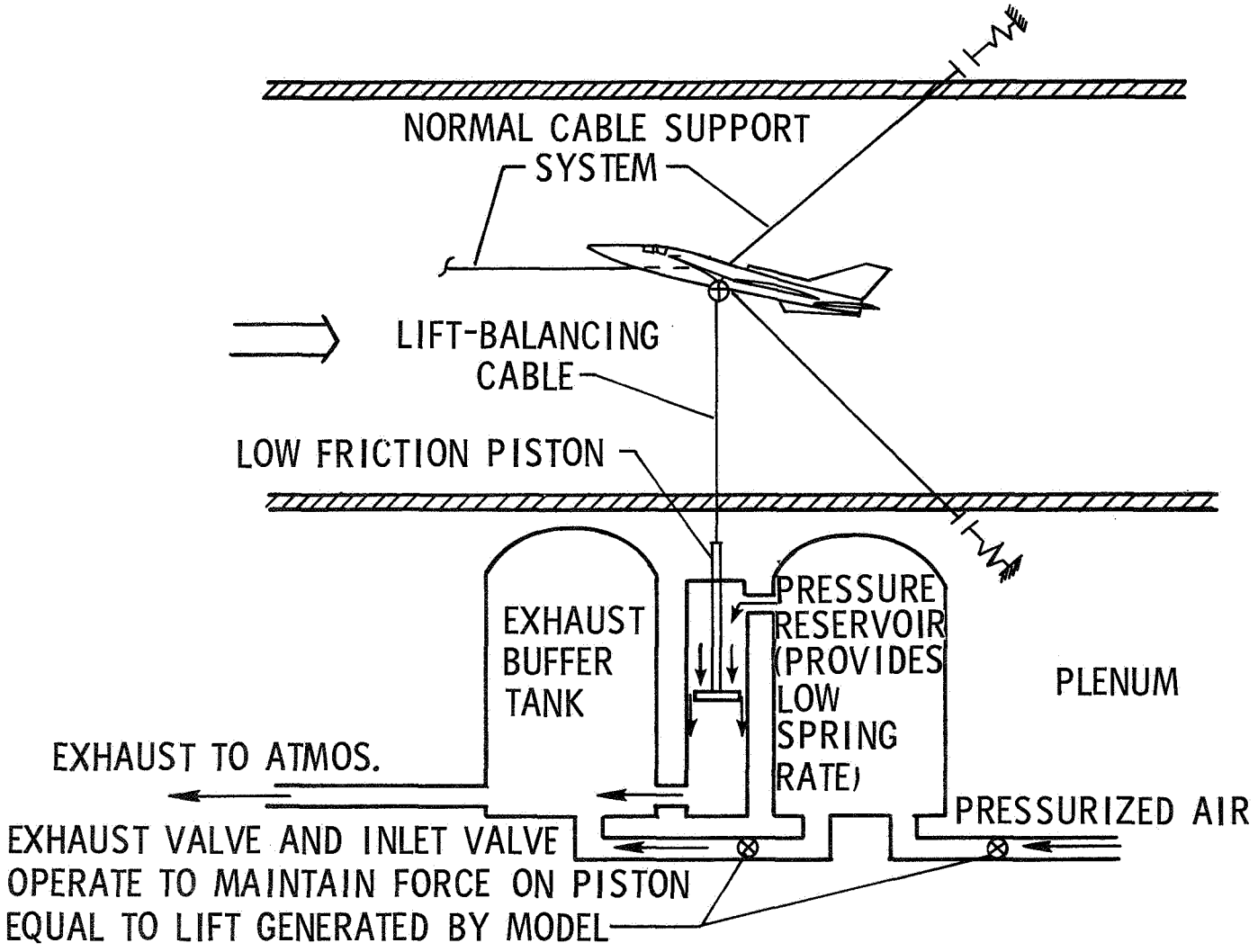

Figure 34.- Schematic diagram of wind-tunnel model lift control device.

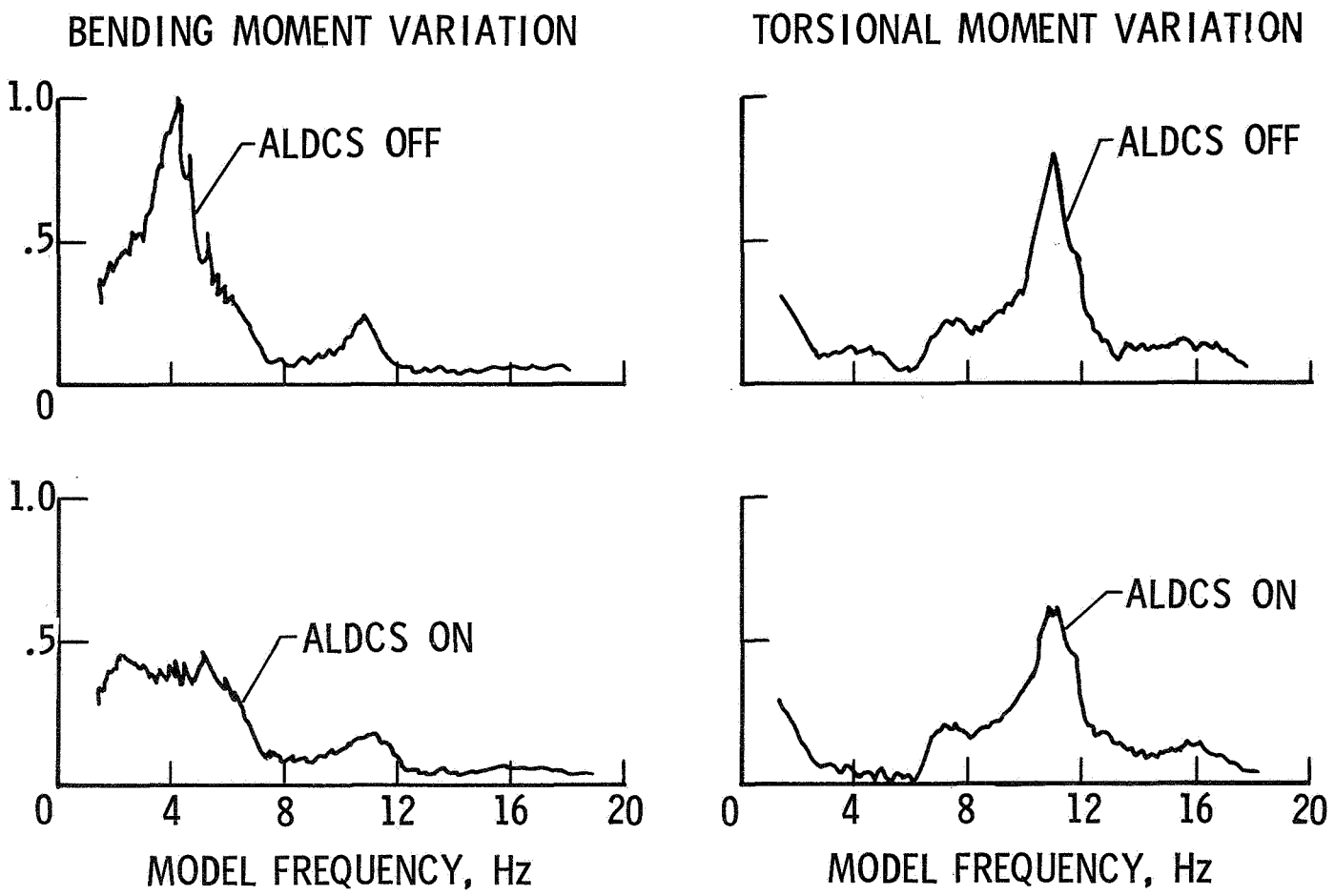

Figure 35.- Variation of C-5A model normalized wing bending and torsional moments with aileron frequency.

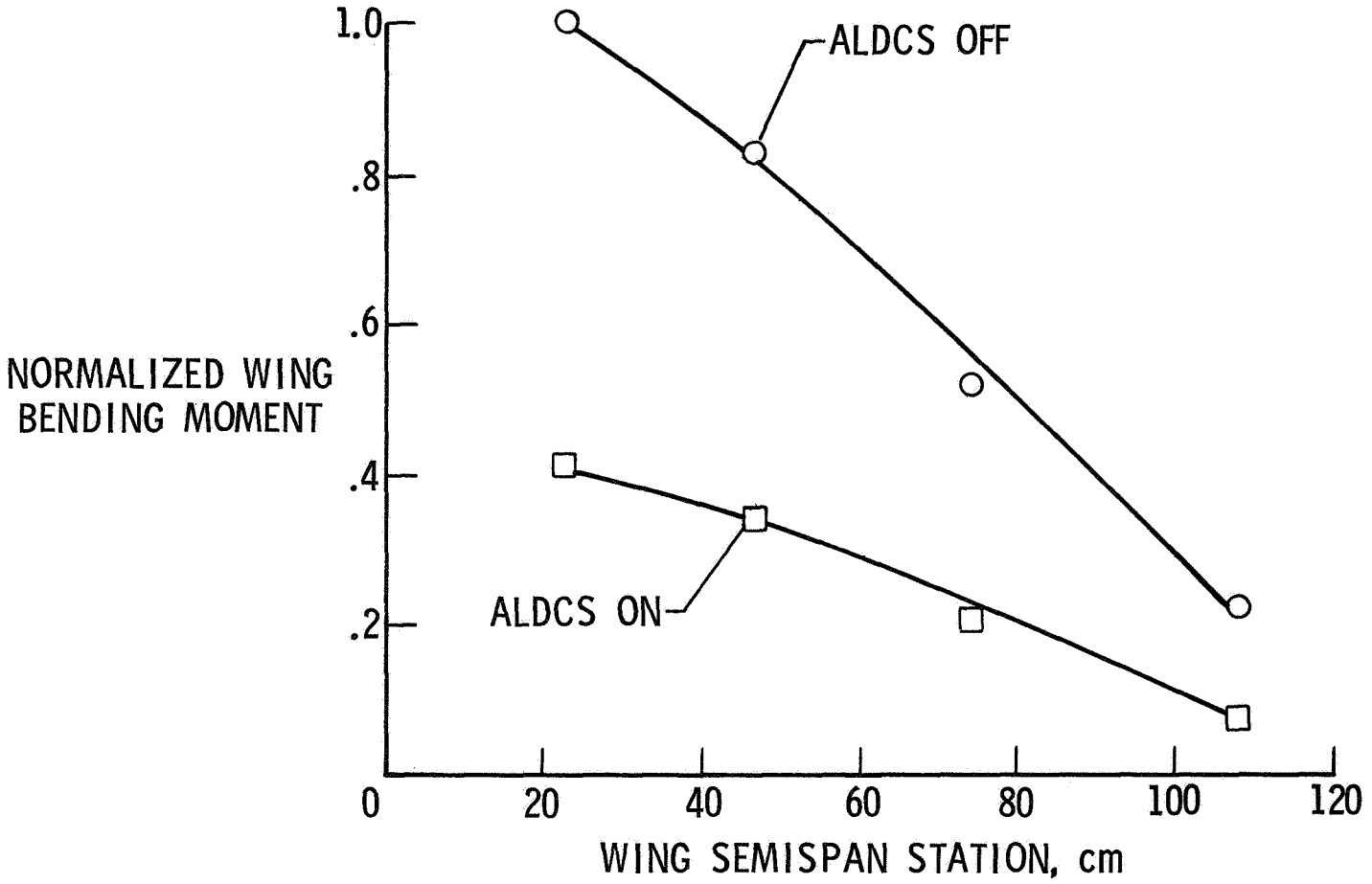

Figure 36.- Spanwise distribution of C-5A model normalized dynamic wing bending moment at a frequency of 4 Hz.

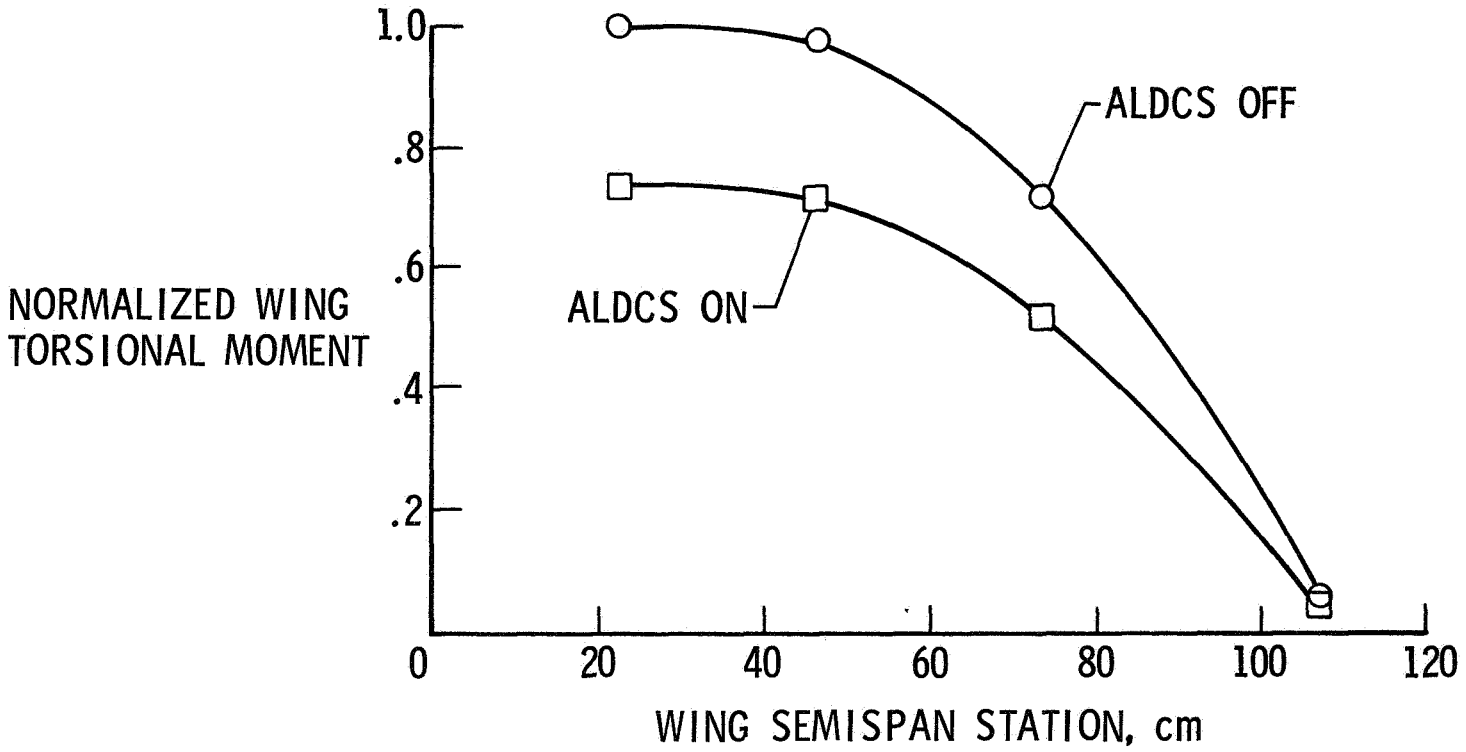

Figure 37.- Spanwise distribution of C-5A model normalized dynamic wing torsional moment at a frequency of 11 Hz.

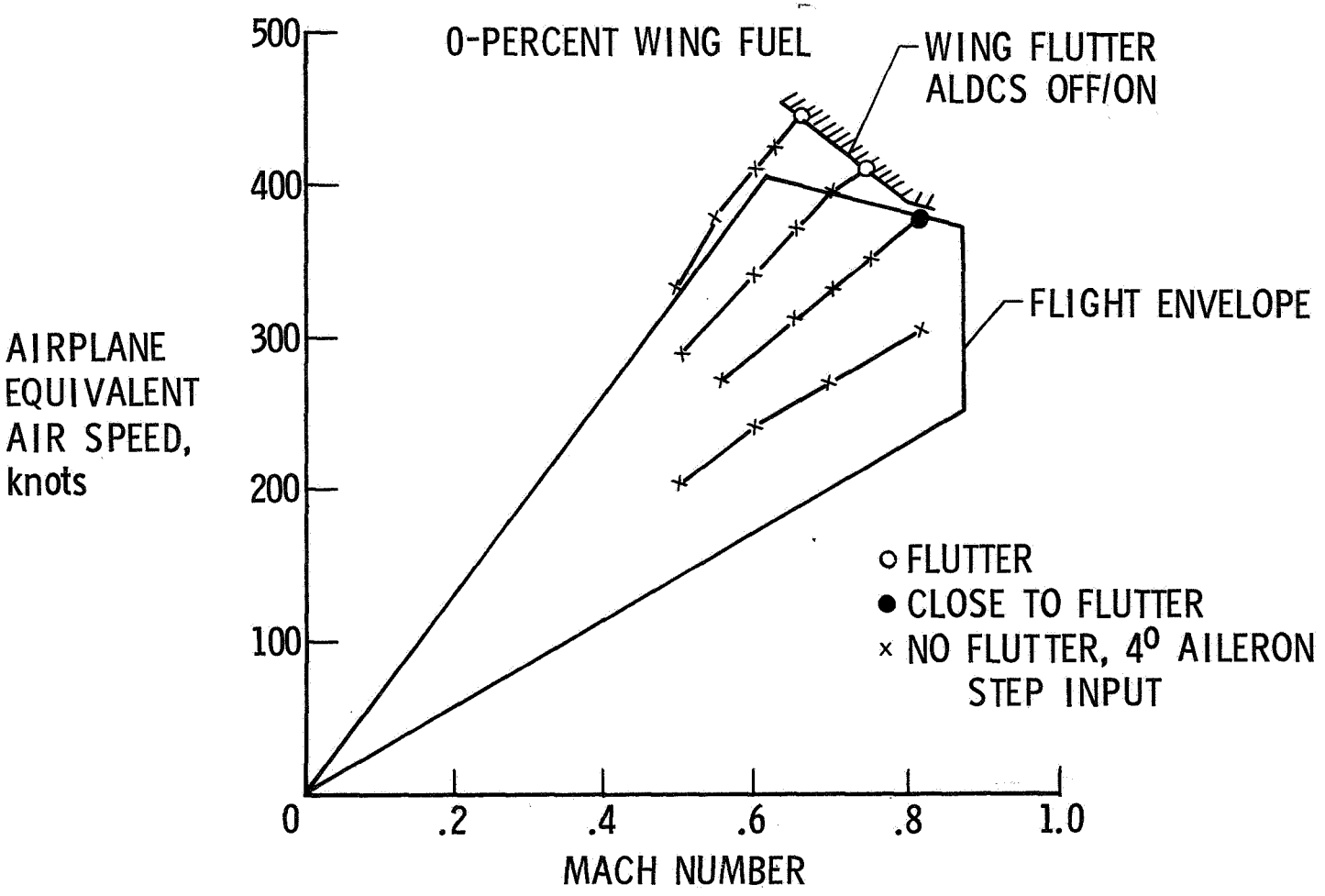

Figure 38.- Effect of ALDCS on C-5A model wing flutter.